NTNU – Trondheim
Norwegian University of
Science and Technology

Microfluidic flow cells for studies of electrochemical reactions

Christine Møinichen

Chemical Engineering and Biotechnology
Submission date: June 2012
Supervisor: Frode Seland, IMTE
Co-supervisor: Per Kristian Dahlstrøm, IMT
David A. Harrington, University of Victoria

Norwegian University of Science and Technology
Department of Materials Science and Engineering

Preface

This work has been performed within the course TMT4900 "Materials Chemistry and Energy Technology, Master Thesis" at the Norwegian University of Science and Technology (NTNU) in Trondheim, Norway. The thesis finalizes the master degree at the Department of Materials Science and Engineering. Part of the thesis is further work from the final project report in the course TMT4500 "Materials Technology, Specialization Project" from December 2011.

I would like to thank my main supervisor Associate Professor Frode Seland for guidance and support through this whole project and the constructive feedback. I would also like to thank my co-supervisor PhD Candidate Per Kristian Dahlstrøm for all his help with the experimental work and constructive feedback.

At last I would like to thank the engineers at the Nanolab for all there help and guidance along the way, and David Barriet, Postdoctoral Fellow at the Department of Physics. Without his help with the SU-8 2100 photoresist I would not have been able to make a higher flow channel with the little time I had left.

I declare that the work has been performed independently and in accordance with the rules and regulations of the Norwegian University of Science and Technology (NTNU).

Christine Møinichen
Trondheim, June 22th 2012

Abstract

In this project the main goal was to establish a routine for making a microfluidic flow cell (MFFC) using soft lithography methods, and test the flow cell with different electrolytes, sulphuric acid and a ruthenium red-ox couple, and eventually use the established routine to make a microfluidic fuel cell and test it.

A routine was established using the negative photoresist ma-N405. The photoresist was overdeveloped to make sure an undercut profile was reached, which proved to be necessary for the subsequent metal lift-off. Titanium (10 nm) and platinum (25 nm) were vapor deposited on the glass chips, and the lift-off process was completed in a couple of days.

Flow channels of two different heights (about 15 and 100 µm) were made by making an impression in PDMS. A low flow channel, height of 15 µm, showed a significant electrolyte resistance in the experimental electrochemical work, and none of the experiments gave the expected results. The electrolyte resistance was measured by electrochemical impedance spectroscopy and taken to be the value corresponding to the high frequency intersection of the real axis. In addition, this resistance was estimated from cyclic voltammetry and taken to be the reciprocal of the slope of the curve, and was found to vary between 10^4-10^7 Ω. The results from EIS and CV were compared, and they overlapped quite well. An MFFC with a channel height of 100 µm and 500 µm electrodes, resulted in a significant decrease in measured electrolyte resistance and gave improved electrochemical results. The electrolyte resistance was measured from EIS and was reduced a lot to about 300 - 10000 Ω. These results were not compared with linear regression of the linear hydrogen area since the hydrogen area was no longer linear.

The cell was tested with a ruthenium red-ox couple (hexaammineruthenium(II)chloride and hexaammineruthenium(III)chloride), and an external hydrogen reference electrode placed in the outlet was found to be simpler to control than an internal reference electrode. The potential limits were -0.3 and 0.3 V vs. an external hydrogen electrode in the same electrolyte. The effect of flow rate, sweep rate and oxygen content in the electrolyte was investigated.

Sammendrag

I denne oppgaven var hovedmålet å etablere en rutine for å lage en mikrofluidteknisk strømningscelle (MFFC) og ved å bruke litografimetoder, og teste strømningscellen med forskjellige elektrolytter, svovelsyre og ruthenium red-ox-par, og til slutt bruke den etablerte rutinen til å lage en mikrofluidteknisk brenselcelle samt foreta testing.

En rutine ble lagd for den negative fotoresisten ma-N 405. Fotoresisten ble overfremkalt for å sikre en undergravd profil som viste seg å være nødvendig under metall-lift-off senere. Titan (10 nm) og platina (25 nm) ble dampdeponert på glassplatene, og lift-off-prosessen ble ferdig på et par dager.

Strømningskanaler ble lagd i to forskjellige høyder (omtrent 15 og 100 µm) ved å lage at avtrykk i PDMS. En lav strømningskanal, 15 µm, viste en betydelig elektrolyttmotstand i det elektrokjemiske eksperimentelle arbeidet, og ingen av forsøkene gav de forventede resultatene. Elektrolyttmotstanden ble målt ved elektrokjemisk impedans spektroskopi og ble gitt verdien som korresponderer til skjæringspunktet mellomhøy frekvens og den reelle aksen. I tillegg ble elektrolyttmotstanden estimert fra syklisk voltammetri og gitt verdien en over stigningstallet til kurven, og ble funnet til å være i området 10^4-10^7 Ω. Resultatene fra EIS og CV ble sammenlignet, og de overlappet svært bra. En MFFC med kanalhøyde 100 µm og 500 µm elektroder resulterte i betydelig redusering av målt elektrolyttmotstand og gav mye bedre elektrokjemiske resultater. Elektrolyttmotstanden ble målt fra EIS og var redusert kraftig til området 300 - 10000 Ω. Disse resultatene ble ikke sammenlignet med lineær regresjon av det lineære hydrogenområdet, da hydrogenområdet ikke lenger var lineært.

Strømningscellen ble testet med et rutenium red-ox-par (hexaammineruthenium(II)chloride and hexaammineruthenium(III)chloride), og en ekstern hydrogen referanseelektrode plassert ved utløpet, ble funnet til å være enklere å kontrollere enn en intern referanse elektrode. Potensialgrensene var -0.3 og 0.3 V mot en ekstern hydrogen elektrode i samme elektrolytt. Effekt av strømningshastighet, sveipehastighet og oksygeninnhold i elektrolytten ble undersøkt.

Table of contents

List of figures

2 Theory

4 Experimental

5 Results

List of tables

List of symbols and abbreviations

AFC	Alkaline Fuel Cell
$c_{x=0}$	Surface concentration [mol dm^{-3}]
$c_{x=\infty}$	Bulk concentration [mol dm^{-3}]
C_{dl}	Capacitance
CE	Counter electrode
CV	Cyclic voltammetry
D	Diffusion coefficient [$cm^2\ s^{-1}$]
d	Diameter [m]
E	Open circuit potential [V]
E^0	Standard potential [V]
EIS	Electrochemical Impedance Spectroscopy
F	Faradays constant, 96485 [C mol^{-1}]
ΔG	Gibbs free energy [J mol^{-1}]
ΔG^0	Standard Gibbs free energy [J mol^{-1}]
HMDS	1,1,1,3,3,3-Hexamethyldisillazane
J	Flux
j	Current density [A cm^{-2}]
jd	Displacement current [A cm^{-2}]
j_D	Disk current density [A cm^{-2}]
jF	Faradic current [A cm^{-2}]
j_R	Ring current density [A cm^{-2}]
j_{lim}	Limiting current density [A cm^{-2}]
K	Equilibrium constant
MCFC	Molten Carbonate Fuel Cell
MFFC	Microfluidic Flow Cell
N_0	Collection efficiency
N_{Re}	Reynolds number
n	Number of electrons transferred [mol]
PAFC	Phosphoric Acid Fuel Cell
PDMS	Polydimethylsiloxane
PEMFC	Polymer Electrolyte Membrane Fuel Cell
R	Universal gas constant, 8.314 [J R^{-1} K^{-1}]
r_1	Disk outer diameter [m]
r_2	Ring inner diameter [m]
r_3	Ring outer diameter [m]
R_S	Electrolyte resistance [Ω]
R_{CT}	Charge transfer resistance [Ω]
RDE	Rotating Disk Electrode
REF	Reference electrode
rpm	Revolutions per minute [rad s^{-1}]
RRDE	Rotating Ring-Disk Electrode
SHE	Standard Hydrogen Electrode
SOFC	Solid Oxide Fuel Cell

T	Temperature [K]
t	Time [s]
V	Volume [mL]
WE	Working Electrode
α	Geometrical constant dependent on r_1 and r_2
β	Geometrical constant dependent on r_1, r_2 and r_3
δ_N	Nernst diffusion layer thickness [m]
υ	Average velocity of the fluid [m s^{-1}]
λ	Wavelength [m]
μ	Fluid viscosity [Pa·s]
ν	Kinematic viscosity [cm^2 s^{-1}]
ρ	Fluid density [kg m^{-3}]
ω	Rotation speed [rad s^{-1}]

1 Introduction

With the energy requirements the world faces today, finding new and more efficient ways to produce energy is important. Not only has the energy demand increased a lot over the last decades, but also the requirements to how the energy is produced have changed. Because of all the climate changes, e.g. global warming, it is very important to reduce the amount of carbon dioxide produced and released to the atmosphere. This has increased the focus on renewable energy sources, like hydrogen and biomass.

Hydrogen is difficult to store in large quantities at room temperature and atmospheric pressure because it is a gas. Very large storage tanks are needed which makes hydrogen unpractical to use as a fuel for instance in cars. Other fuels like methanol, ethanol and formic acid are liquids at room temperature and atmospheric pressure and much more easy to store and handle in large quantities. The downside is a slower and more complicated electrode kinetic.

Today, platinum is one of the most common catalysts. Platinum is a very rare element, which makes it expensive to use. Platinum is often used as a catalyst in fuel cells due to the harsh environment introduced by the electrolyte used (acid based fuel cells). A fuel cell converts chemical energy to electrical energy, and some heat. Several types of fuel cell technology exist today (PEMFC, AFC, PAFC, MCFC and SOFC) distinguished by the active electrolyte used leading to various temperature windows of operation, range of application (in Watts) and usable fuels (purification demands). However, as a general rule they all need an ionic separator that prevents the reactions from reacting chemically and force electrons to move in an outer circuit. Typically, this is done with the introduction of a thin ionic conducting material.

The possibilities for microfluidics are many, for instance with fuel cells, in studying unknown and complicated electrode kinetics and development of biological catalysts (enzymes, bacteria) and metallic catalysts, [1]. The MFFC is desirable for mainly three reasons, (i) the removal of the membrane in a fuel cell reduces the cost significantly, (ii) can be used to understand electro catalytic reactions and (iii) often small amounts of catalyst is needed and can be expensive to make, therefore, the MFFC is beneficial to use. Since the flow is laminar in a MFFC, two different electrolytes can flow side by side through the same channel without mixing. The composition of the anodic and cathodic streams can be chosen independently and therefore improve the reaction rates and cell voltage. This also means that for a cell with two working electrodes, the electrolyte will have to be liquid, and not gas to maintain ionic conductivity between the electrodes.

The purpose of this project has been to establish a routine for making MFFCs of any design depending on processing parameters like type of photoresist, rotation speed, exposure time, development time and the thickness of the vapour deposited metal layer by using soft lithography methods. The flow channel is made from PDMS, polydimethylsiloxane. After establishing an experimental procedure to prepare microfluidic flow cells, the cells are here used for electrochemical experiments with support electrolyte to verify their adequacy. Operational parameters like flow rate, electrode positioning, channel height and oxygen are tested with and without the presence of a Ru salt red-ox couple (hexaammineruthenium(II)chloride / hexaammineruthenium(III)chloride).

A final objective has been to design a new photomask in AutoCAD with electrode and flow channel pattern for a microfluidic fuel cell.

The long term goals for the Electrochemical Energy Group at the Department of Material Science and Engineering, is to use the MFFC as a standard technique for increasing the knowledge of electrocatalysis of distinct systems related to fuel cells and water electrolysis, and at the same time offer the possibility for interdisciplinary collaboration at NTNU, e.g. with biotechnology in the development of biological catalysts.

2 Theory

Fuel cells have become popular over the last couple of decades due to their improved efficiency and exhaust characteristics than the internal combustion engine. Incorporating the use of fuel from renewable sources has paved the way for numerous studies on all aspects of the fuel cells with the ultimate desire of a more environmentally friendly society. The intensive studies over the years have led to development of several types of fuel cells, where PEMFC, AFC, PAFC, MCFC and SOFC are the most important ones. In particular PEMFC, operating at temperatures between ambient and up to 100 °C have gained attention from most of the car manufactures and represent a viable alternative to the internal combustion engine driven cars. The major drawbacks that prevent full scale commercialization are (i) the expensive parts that PEMFCs consist of, i.e. noble metal catalyst (Pt metals), membranes and bipolar plates, (ii) life time of the fuel cell, i.e. it has to be able to operate a certain amount of hours, and (iii) the fuel that such systems use is limited, usually need extensive pre-treatment, calls for new regulations (i.e. health and safety) as well as a lacking infrastructure. A lot of work has been done on the political level to increase the acceptance of alternative energy devices and fuels (e.g. fuel cells and hydrogen, and Li-batteries), but a lot of work still remain.

2.1 Hydrogen Fuel cells - basic principles

A fuel cell converts chemical energy to electrical energy. In a hydrogen-based fuel cell, e.g. the PEMFC, hydrogen gas is fed at the anode and is burned or combusted through the reaction with oxygen gas fed at the cathode, see reaction 3.1, [2].

$$H_2 + ½O_2 \rightarrow H_2O \qquad (2.1)$$

The current produced is rather small, and the main reasons are first the low contact area between the gas, the electrode and the electrolyte and second the large distance between the electrodes. Reaction 2.2 release electrons and produces H^+ ions which reaction 2.3 needs. The H^+ ions pass through the electrolyte, and it is important to make sure that only the H^+ ions and not the electrons passes through the electrolyte. If not, the electrons would go through the electrolyte instead of an external circuit.

There are four reasons for the voltage drop in a fuel cell, and they are activation losses, fuel crossover and internal currents, ohmic losses and mass transport or concentration losses. For a fuel cell operating below 100 °C, the theoretical cell voltage is usually about 1.2 V (slightly temperature dependent). As seen in figure 3.1 the open circuit voltage is below the theoretical cell voltage. This is due to activation losses caused by the slow reaction taking place on the electrode surface, which gives initially a rapid fall in cell voltage.

The electrolyte should only transport ions and not electrons. However, some fuel diffusion and electron flow will be possible. The linear region in figure 2.1 is due to ohmic losses. The ohmic voltage drop is because of the resistance to the flow of electrons through the

interconnections and the resistance to the flow of ions through the electrolyte, where the latter is the most significant.

At the end of the linear ohmic drop region there is a sudden and distinct decrease in the cell voltage due to mass transport. Mass transport losses are related to the consumption of reactants, see reaction 2.1.

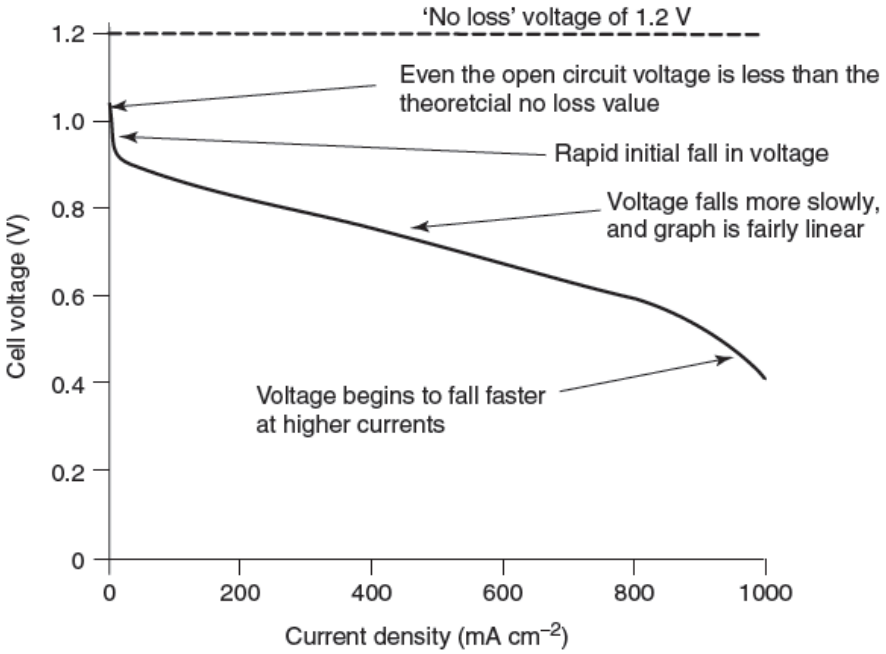

Figure 2.1: Cell voltage as a function of current density for a fuel cell at low temperature and air pressure, [2].

In a Polymer Electrolyte Membrane Fuel Cell, PEMFC, the electrode reactions are

$$\text{Anode: } H_2 \rightarrow 2H^+ + 2e^- \qquad E^0 = 0 \text{ V} \qquad (2.2)$$

$$\text{Cathode: } \tfrac{1}{2} O_2 + 2H^+ + 2e^- \rightarrow H_2O \qquad E^0 = 1.23 \text{ V} \qquad (2.3)$$

The total cell reaction is equal to equation 2.1. The Nernst equation can be derived from the relationship between Gibbs free energy and standard Gibbs free energy

$$\Delta G = \Delta G^0 + RT\ln Q \qquad (2.4)$$

where ΔG is Gibbs free energy, ΔG^0 is Gibbs free energy at standard pressure and temperature and with pure reactants, R is the gas constant, T is the temperature in Kelvin and Q is the reaction quotient. ΔG can be expressed as

$$\Delta G = -nFE^{rev} \qquad (2.5)$$

where n is the number of electrons transferred, F is Faradays constant 96485 $Cmol^{-1}$ and E^{rev} is the reversible potential. By inserting equation 2.5 into 2.4 the following expression is obtained

$$-nFE^{rev} = -nFE^{0} + RTlnQ \quad (2.6)$$

E^0 is the potential at standard pressure and temperature and with pure reactants. Equation 2.7 can be rewritten as

$$E^{rev} = E^{0} - \frac{RT}{nF} lnQ \quad (2.7)$$

This equation is called the Nernst equation.

Reference electrodes

There are several types of reference electrodes, and the electrode potential is dependent on the ion concentration (if ions are a part of the electrode reaction), [3].

For the hydrogen reference electrode the reaction quotient is a function of the hydrogen ion concentration. This shows that the potential is pH dependent, which means by changing the pH the potential also changes. In the electrode reaction two electrons is transferred, n =2, and at room temperature, T = 298.15 K, and by using standard mathematical rules for the natural logarithm, equation 2.7 can be written as

$$E^{rev} = E^{0} - 0.059 \cdot pH \quad (2.8)$$

This means that the reference potential will decrease with increasing pH.

Another reference electrode is the silver/silver chloride electrode. Here the reaction quotient is dependent on the chloride concentration, and the potential will decrease with increasing chloride concentration, see equation 2.9.

$$E^{rev} = E^{0} - \log(a_{chloride}) \quad (2.9)$$

The potential difference between the hydrogen electrode and the silver/silver chloride electrode is 0.2224 V vs. SHE.

2.2 Mass transport in electrochemical systems

The flux of a dilute species *i* will depend on migration, diffusion and convection, see equation 2.10, [4].

$$J_i = J_i^M + J_i^D + j_i^C = -z_i F u_i c_i \nabla\Phi - D_i \nabla c_i + c_i \nu \quad (2.10)$$

Migration flux is the product of concentration of species *i* and the migration velocity of species *i*. The migration velocity is a function of the mobility of specie *i* and the electric field. When an excess of supporting electrolyte is used, the conductivity of the electrolyte is improved and the migration term in equation 2.10 becomes negligible. The diffusion flux of specie *i* is given by Fick's first law, and is dependent on the diffusion coefficient of specie *i* and the concentration of specie *i*. In the absence of concentration gradients, e.g. well stirred solutions, the diffusion term in equation 2.10 becomes negligible. Convection is because of mechanical stirring, agitation or flow of the electrolyte, and is very complex. By the application of a diffusion layer approximation, described later in subchapter 2.5, the flux calculation can be simplified.

2.3 Microfluidic flow cells (MFFCs)

Microfluidics is defined as "the science and technology of systems that process or manipulate small (10^{-9} to 10^{-18} litres) amounts of fluids, using channels with dimensions of tens to hundreds of micrometers", [5]. Microfluidic devices represent a rather new technology, and was invented in 2002 by Choban et al. [6]. The vast majority of published work on microfluidics has so far been related to chemical engineering and molecular biotechnology. A microfluidic device is defined as a cell with micrometer dimensions. Delivery and removal of electrolyte, reaction sites and electrode structures are all confined within a single microfluidic channel and its walls.

2.3.1 Brief description of flow pattern in a microchannel

The flow is dependent of the Reynolds number and can be calculated from equation 2.11, [7]. The Reynolds number gives an indication whether the flow will be laminar or turbulent.

$$N_{Re} = \frac{d v \rho}{\mu} \quad (2.11)$$

Where *d* is the diameter in meter, ρ is the fluid density in kg m^{-3}, μ is the fluid viscosity in Pa·s and *v* is the average velocity of the fluid in m s^{-1}. If the channel is straight and circular, the flow will be laminar if the Reynolds number is less than 2100. If the Reynolds number is larger than 4000, the flow will be turbulent, and two electrolytes will be mixed when they flow through the same channel. The region between laminar and turbulent is called the transition region, and there is no way to predict what will happen there. It depends on the geometry and the details in the apparatus, and either turbulent or viscous flow is obtained, [7]. A sketch of turbulent and laminar flow is shown in figure 2.2.

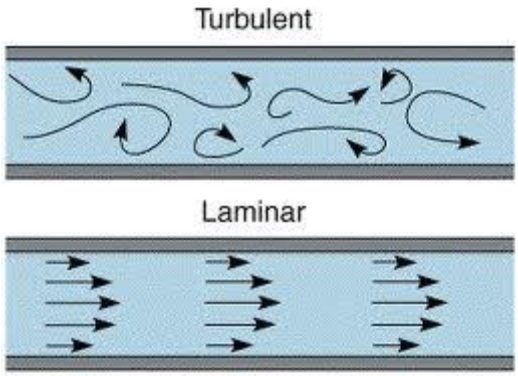

Figure 2.2: Sketch of turbulent and laminar flow, [8].

Most common microfluidic cells will encompass a low Reynolds number in the microchannel flow and therefore yield laminar flow characteristics. Several possible configurations of microfluidic device exist, and will be described briefly in the following subchapters.

2.3.2 Microfluidic fuel cells

First of all, since the low Reynolds number in microchannel flow give laminar flow characteristics and delay convective mixing of reactants, two different electrolytes can flow side by side through the same channel without significant mixing. The composition of the anodic and cathodic streams can be chosen independently and therefore improve the reaction rate and cell voltage. This configuration is typically referred to as a microfluidic fuel cell. Allowing the microfluidic fuel cell to operate with two parallel streams across the electrode structures, the demand for an ionic conducting membrane can be removed. Interdiffusion is limited to a narrow width at the interface in the centre of the channel. Avoiding the membrane requirement reduces the cost of such a fuel cell design significantly. In addition, since the operating temperature is at room temperature, there is no need for a cooling system, water management or supplementary humidification, [9], [10].

Because of the given dimensions laminar flow is achieved, which means that two electrolytes will not be mixed even though they flow though the same channel. Figure 2.3 gives the most common design for microfluidic fuel cells, with various purposes (e.g. flow through electrodes, air breathing electrodes and array of electrodes (stack)). Common for all designs is that there is no physical barrier (membrane) separating the fuel and oxidant.

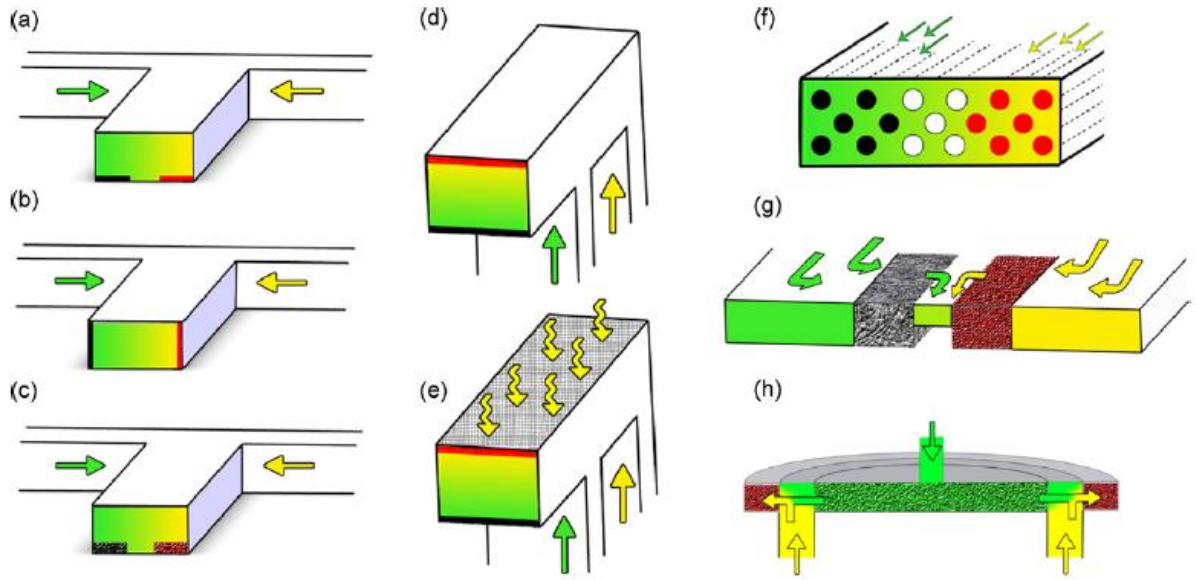

Figure 2.3: Different channel configurations. The fuel is in green, the oxidant is in yellow, anode in black and cathode in red. Figures a), b) and c) have a T-shaped flow channel, and the electrodes are placed on the bottom, on the side and porous electrodes on the bottom respectively. Figures d) and e) have an F-shaped flow channel. The electrodes in figure e) are porous to facilitate air breathing. Figure f) has an array of electrodes, figure g) has a flow through porous electrode and figure h) has a radial porous electrode, [1].

The Microfluidic Flow Cell operates at room temperature, i.e. it is liquid based. If hydrogen and oxygen gas is to be used it would have to be dissolved in the electrolyte. The electrolyte can be acidic or alkaline, so when the two electrolytes flow together in the channel the relationship between the electrolytes could be acid-acid, acid-base or base-base.

An example of a microfluidic fuel cell design is shown in figure 2.4. The flow channel is T-shaped with two inlet holes and one outlet hole. In this example, the channel just covers the two electrodes, but it is possible to use a wider cannel. The active electrode length is the length of electrode inside the channel from where the electrolytes enters the channel.

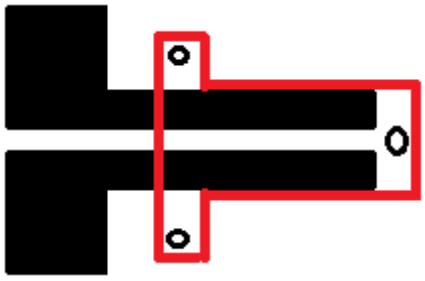

Figure 2.4: Sketch of a microfluidic fuel cell, [9].

The laminar flow prevents two electrolytes from mixing, and the inter-diffusion between the two electrolytes is confined to an hourglass-shaped zone, [9], see figure 2.5. With the appropriate space between the electrodes, fuel and oxidant crossover is limited.

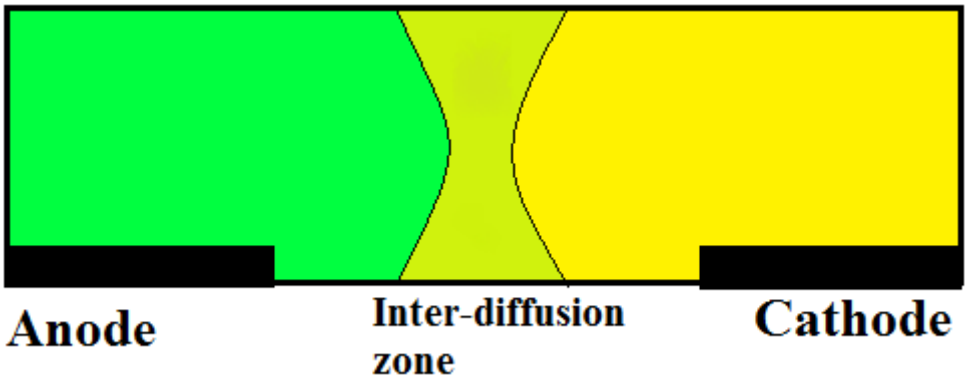

Figure 2.5: Schematic cross-section of the channel shows the co-laminar flow with the inter-diffusion zone.

2.3.3 Multielectrode microchanneled electrochemical cell

Figure 2.6 shows a simple sketch of a Microfluidic Flow Cell with four electrodes placed in the microchannel. The reaction being studied takes place at the first electrode (WE), and the amount of product is subsequently detected at the following three electrodes. The four electrodes can be controlled independently, and can be set at different voltages.

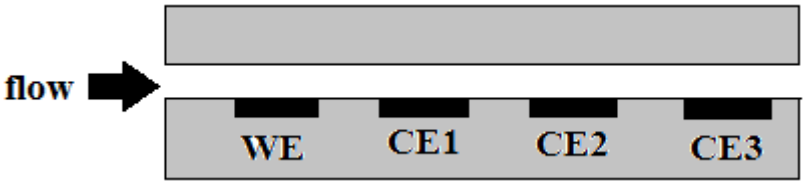

Figure 2.6: Simple sketch of the microfluidic flow cell.

The configuration allows us to study complicated electrochemical reactions, and be able to quantify product formation as well as giving time resolved information of eventual short-lived soluble intermediates, which is more difficult to detect in large electrolyte compartments. It is easy to change the potential at the electrodes, and allows for rapid exchange of the electrolyte if needed. One example of how the MFFC could be used is hydrogen evolution. Hydrogen gas is produced on the first electrode, and the three electrodes downstream are used to detect how much hydrogen that was produced. The working principle is very similar to the well-known rotating ring-disk electrode. A rotating ring-disk electrode (RRDE) only has one ring to detect hydrogen, but the MFFC has three electrodes to detect hydrogen. The electrodes in a MFFC are closer to each other than the ring and disk are on a RRDE. In addition, because of the small channel dimensions less hydrogen will be able to diffuse to the bulk without being detected. Another more sophisticated reaction to study is the electrochemical oxidation of ethanol, that due to the possible transfer of 12 electrons have several possible reaction pathways.

Rather recently, various groups employed a two-electrode system to study Pt dissolution, [11], oxygen reduction, [12], CO oxidation, [13], methanol oxidation, [14], and ethanol oxidation, [15]. However, PDMS alternatives (machined acrylic, Kel-F or PEEK) were used in these studies, which have less flexibility in fabrication, but improved temperature and chemical stability.

As pointed out by Kjeang et al., [16], a cell design with several electrodes confined to a microfluidic flow channel can allow for a more elegant configurations in terms of miniaturization by placing all three electrodes i.e. working, reference and counter electrode, on-chip (inside the channel). This electrode design makes shielding of subsequent electrodes possible. A reactive component is added to the electrolyte flow, for instance carbon monoxide (CO (aq)), and by applying the appropriate potential to the first electrode the electrolyte should be cleansed of this component. The degree of cleansing will depend on the flow rate. Kjeang et al, [16] simulated the concentration profile of the reactive component as a function of flow rate in a microfluidic flow cell. At higher flow rates the active component is transported over the electrode without being completely consumed.

Finally, a microfluidic flow cell can be used to aid understanding and development of a new generation of biological catalysts (enzymes, bacteria) and advanced metallic catalysts. In development of biological catalyst, it is necessary with small dimensions since very small amounts of catalyst are used, and the enzymes can only survive under certain conditions.

2.3.4 Ruthenium salt red-ox couple

The ruthenium red-ox couple hexaammineruthenium(II)chloride and hexaammineruthenium(III)chloride has a formal red-ox potential of E^0 = -0.15 V vs. a silver/silver chloride reference electrode, [16], and the red-ox reaction is

$$Ru(NH_3)_6^{3+} + e^- \leftrightarrow Ru(NH_3)_6^{2+} \tag{2.12}$$

This is a fast reaction, meaning there are no restrictions regarding charge transfer which means that the reaction is diffusion controlled. The Nernst diffusion potential-current behavior, voltammogram, is explained by Fick's first law (subchapter 2.5) when the reaction is diffusion controlled.

In cyclic voltammetry the potential is swept between an upper and lower limit. At zero over-potential the current is zero, and as the potential increases the current increases (concentration gradient increases) until all species are oxidized and the electrode surface concentration is zero. At zero surface concentrations the current reaches a maximum value (the peak in the voltammogram). All molecules who reach the working electrode react immediately and the current is limited by the diffusion of reactant to the electrode, [16]. Even though the potential is increased the current is reduced because the concentration gradient decreases. When the potential is swept down again, the same happens, only its reduction of the species and not oxidation, and when all species are reduced the surface concentration is again zero, and a low

point appears in the voltammogram. If the potential is reduced, the current increases because of increasing concentration gradient.

At steady stat, the Nernst diffusion layer thickness is independent of time and the potential-current behavior is altered compared to the diffusion controlled scenario. Since the Nernst diffusion layer thickness is constant, the concentration gradient reaches a maximum when the electrode surface concentration reaches zero, and the current will flatten at higher potentials.

In systems with rotation or flow the Nernst diffusion layer thickness will decrease with increasing rotation or flow rate and a higher current is expected, [16].

When choosing a supporting electrolyte, there are some considerations to be made, like the possibility of interferences with the process chemistry of the system, [16]. There are many red-ox couples and supporting electrolytes to chose from, and they are tabulated by Bard et al., [17].

Potassium sulphate (K_2SO_4) is chosen as a supporting electrolyte, instead of an acidic electrolyte, because of the order of maximum separation of the Ru salt red-ox couple and the hydrogen red-ox potentials, [16].

2.4 Cyclic voltammetry

When performing cyclic voltammetry the upper and lower limit for the potential is set depending on the electrolyte and the reaction taking place. The potential is swept between the given limits N number of cycles. The convention used is that positive going current is anodic, and negative going current is cathodic. Usually the potential limits E_t^a and E_t^c are chosen to be the potential for hydrogen and oxygen evolution, se figure 2.7, in aqueous electrolyte. By using metals like platinum and gold it is possible to get reproducible results, when scanning between these limits. The different metals give very different voltammograms, [18].

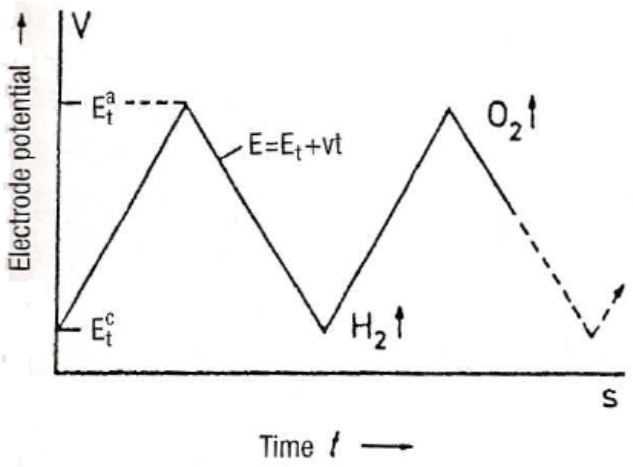

Figure 2.7: Electrode potential as a function of time at the working electrode, [18].

A cyclic voltammogram, figure 2.8, can be used to calculate the electrode area. A monolayer of hydrogen is adsorbed on the electrode surface, i.e. only one hydrogen atom is adsorbed per platinum atom on the electrode surface. By calculating the number of charges in the hydrogen adsorption region and dividing that number with the platinum charge per cm^2, 220 μC $cm(Pt)^{-2}$, [19], the electrode area is obtained. For a more detailed description, see appendix A.

2.4.1 Pt electrode in the presence of sulphuric acid with Ar (g) purging

When there are no dissolved active species in the electrolyte like oxygen or hydrogen, due to argon or nitrogen gas purging, a current potential behaviour (voltammogram) like the one in figure 2.8 is observed. This voltammogram represents only surface reactions between platinum and water and eventual anion interactions (0.5 M H_2SO_4).

The butterfly peaks in the lower potential region (0-0.4 V) represents the hydrogen region where the negative current peaks are hydrogen adsorption according to reaction 2.13. The positive peaks in the positive going scan represents the hydrogen desorption which is reaction 2.13 in reverse.

$$Pt + H^+ + e^- \rightarrow Pt\text{-}H \qquad (2.13)$$

At potentials more positive than the hydrogen region, the current is low and constant until about 0.7 V, where only charging/discharging of the double layer occurs. This region is therefore commonly referred to as the double layer region. At potentials above 0.75 V in the positive-going scan, the current increase and one enters the oxide region where platinum oxide is being formed, first according to reaction 2.14 and subsequently further oxidation according to reaction 2.15. The formation of platinum oxide is rather complicated and many studies have been done to understand the kinetics behind its origin

$$Pt + H_2O \rightarrow Pt\text{-}OH + H^+ + e^- \qquad (2.14)$$

$$Pt\text{-}OH \rightarrow Pt\text{-}O + H^+ + e^- \qquad (2.15)$$

As opposed to the hydrogen adsorption/desorption, which is highly reversible, oxide films on noble metals are found to be irreversible. Oxide films formed at higher potentials need a lower, less positive, potential to reduce the oxide film formed. This is independent of the potential sweep rate, [20]. At potentials higher than 1.6 V, oxygen evolution takes place according to reaction 2.16.

$$2H_2O \rightarrow O_2 + 4H^+ + 4e^- \qquad (2.16)$$

When the potential sweep is reversed, any oxygen present in the electrolyte will be reduced along with the chemisorbed oxide-film. At lower potentials, there is still a small double-layer region, and this is followed by the adsorption of hydrogen again according to reaction 2.13.

When the potential is close to the reversible potential for the H_2/H_2O couple, there is a strong hydrogen evolution, which can be reversed if the potential sweep changes direction. In figure 2.8 the lower potential limit is fixed to be just before this onset of hydrogen evolution.

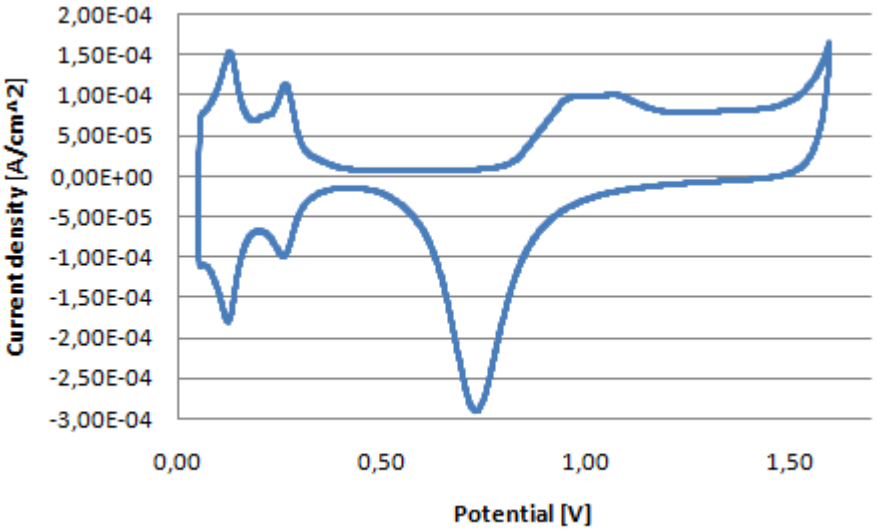

Figure 2.8: Cyclic voltammogram of platinum electrodes in 0.5 M H_2SO_4, and argon purging. There is no rotation and the potential sweep rate is 100 mV/s. Lower potential limit is 0.05 V and upper potential limit is 1.6 V.

2.4.2 Effect of oxygen present in the electrolyte

The presence of oxygen in the electrolyte adds a negative contribution to the current, due to film formation on the electrode, [18], in the hydrogen region and the double layer region but the oxygen region is the same for both voltammograms, see figure 2.9. At low potential sweep rates the oxygen contribution can be neglected and the CV will be similar to the quasi-stationary current-potential response for oxygen reduction, but at much higher potential sweep rates the presence of oxygen is more dominating. The film formation and dissolution is independent of the oxygen reduction.

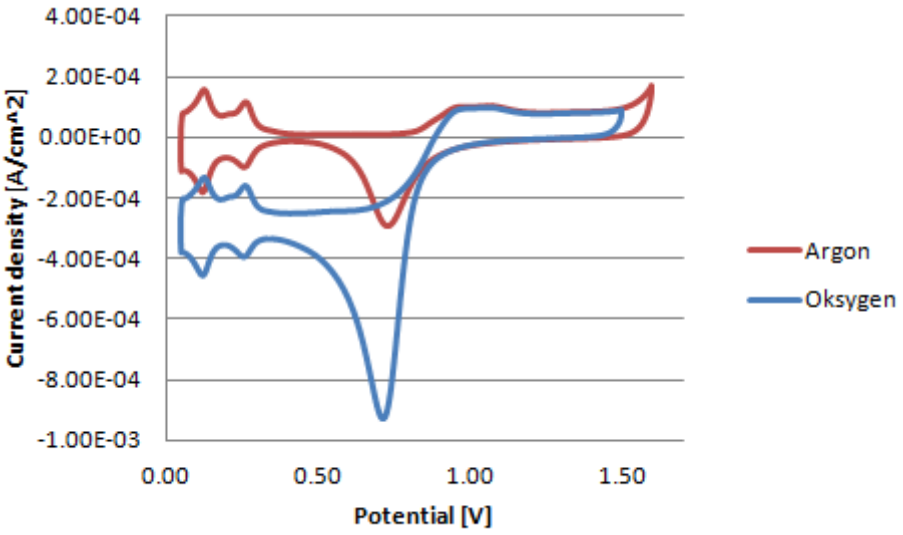

Figure 2.9: Cyclic voltammetry with platinum electrodes in 0.5 M H_2SO_4 with both argon purging and oxygen purging. The potential lower limit was 0.05 V and the upper potential limit was 1.5 /1.6 V. There was no rotation, $\omega = 0$ rpm, and the potential sweep rate was 100 mV s^{-1}.

2.5 Rotating disk electrode and rotating ring-disk electrode

The rotating disk electrode, figure 2.10, is of great importance. The electrode, which is the working electrode, rotates with a given angular velocity ω, and when rotating the liquid is drawn up along the rotating axis to the disk and then flung outwards. Figure 2.11 a) is a schematic presentation of a rotating disk electrode, figure 2.11 b) shows the azimuthal flow at the disk during rotation and figure 2.11 c) shows how the liquid is drawn up to the disk.

Figure 2.10: Picture of a RDE, [21].

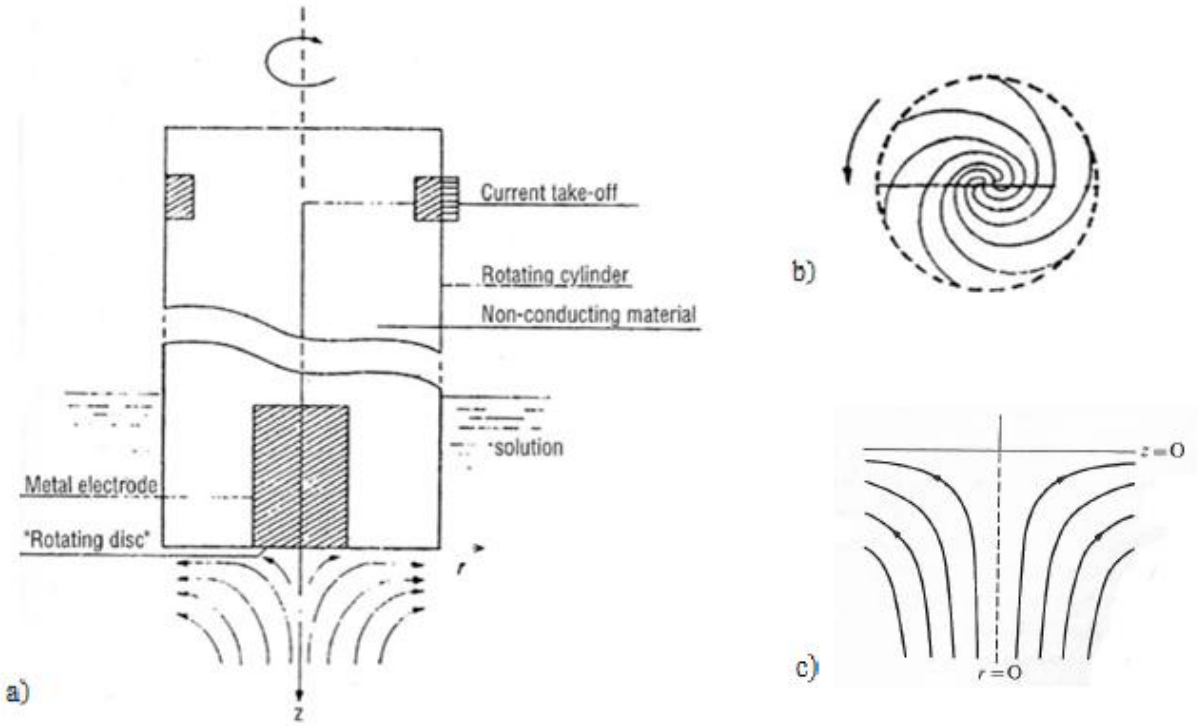

Figure 2.11: a) Schematic presentation of a rotating disk electrode, b) shows the azimuthal flow during rotation, [18], and c) shows how the electrolyte is sucked upwards when the RDE is rotating, z=0 is the electrode surface, [22].

If a reaction is diffusion controlled it means that the molecules are moving without external influence. The molecules diffuse from a high concentration region to a low concentration region. This difference in concentration is usually named the concentration gradient, but diffusion can take place even if there is no concentration gradient present. Diffusion is not an equilibrium state and the diffusion will take place until equilibrium is reached, the concentration is equal in both regions. The diffusion coefficient tells how fast the molecules diffuse. A simple way to look at it is the Nernst diffusion layer with thickness δ_N at the surface, see figure 2.12 for an example, [4].

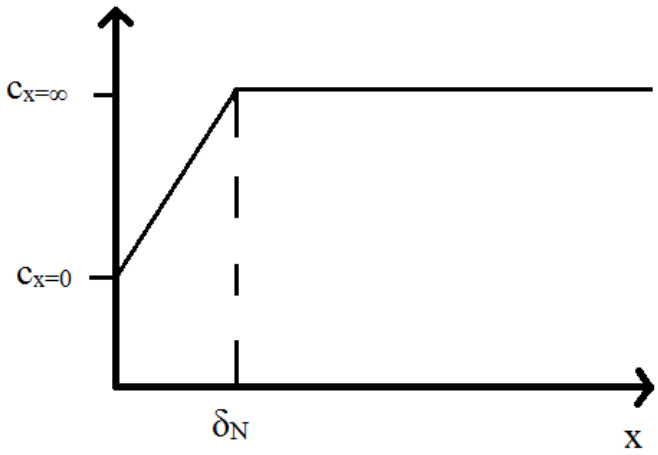

Figure 2.12: Concentration profile with Nernst diffusion layer thickness. Here the surface concentration is not zero, i.e. not limiting current region.

One assumption made is that in the Nernst diffusion layer only diffusion contributes to the mass transport. Outside this layer it is assumed that convection is the main contributor to mass transport (migration is ignored in the presence of a supporting electrolyte). Convection is due to mechanical stirring, agitation or flow of the electrolyte. The bulk of the electrolyte is assumed to be well mixed, and therefore the concentration gradients are confined to a thin diffusion layer adjoining to the electrode surface, [4].

Fick's first law describes diffusion, and for one dimensional diffusion through a planar surface the expression is [18]

$$J_i = -D_i\left(\frac{dc_i}{dc_x}\right) = \frac{j}{nF} \tag{2.17}$$

J_i is the diffusion flux of component *i*. This equation can be rewritten and give an expression for the current density

$$j = nFD\left(\frac{\partial c}{\partial x}\right)_{x=0} = nFD\frac{c_{x=\infty} - c_{x=0}}{\delta_N} \tag{2.18}$$

As the surface concentration approaches 0, $c_{x=0} \rightarrow 0$, the limiting current is obtained

$$j_{lim} = nFD\frac{c_{x=\infty}}{\delta_N} \tag{2.19}$$

If there is no rotation the reaction is diffusion controlled, and the limiting current will decay as a function of time according to Cottrell's equation, equation 2.20.

$$j_{lim} = nFD^{\frac{1}{2}}c_{x=\infty}\frac{1}{\sqrt{\pi t}} \tag{2.20}$$

On the other hand, if rotation is applied to the rotating disk electrode, the limiting current density is no longer a function of time, but depends instead on how fast the disk is rotating, and can be expressed as:

$$j_{lim} = \frac{nFDc_{x=\infty}}{\delta_N} = -0.62nFAD^{\frac{2}{3}}\nu^{-\frac{1}{6}}\omega^{\frac{1}{2}}c_{x=\infty} = B\omega^{\frac{1}{2}} \tag{2.21}$$

where the Nernst diffusion layer thickness $\delta_N = 1.61D^{\frac{1}{3}}\nu^{\frac{1}{6}}\omega^{-\frac{1}{2}}$ and B is a constant. Equation 2.21 is called the Levich equation. The diffusion coefficient can be determined from the slop of the straight line obtained by plotting the limiting current density as a function of the square root of the rotation speed and forcing it through zero. If the diffusion coefficient is known, the bulk concentration can be found in a similar manner and is sometimes used analytically to determine bulk concentration of dissolved species. Figure 2.13 a) shows how the limiting current density varies with the rotating speed, while figure 2.13 b) is an example of a Levich plot with an extrapolated straight line to the origin.

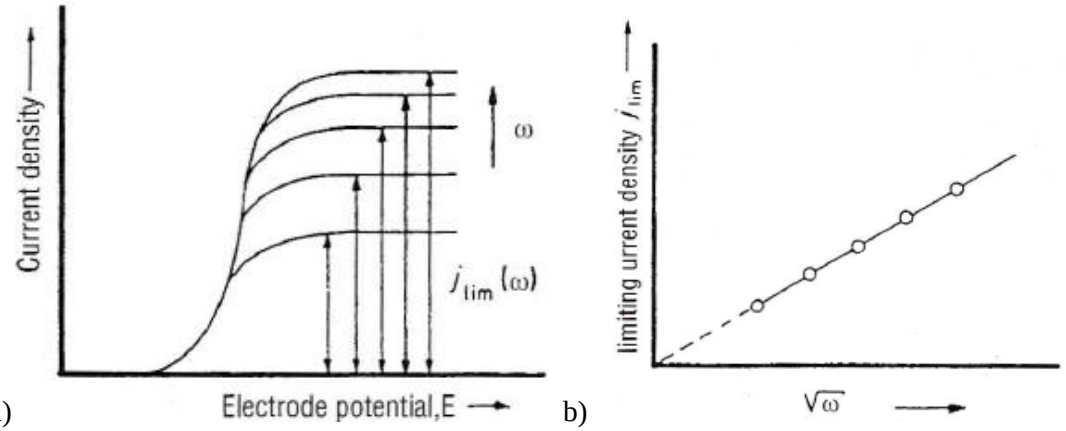

a) b)

Figure 2.13 a) Current density as a function of electrode potential, and b) limiting current density as a function of the square root of the angular velocity, [18].

Rotating ring-disk electrode

The rotating ring-disk electrode has two independent electrodes, a disk and a ring, and they are separated by a concentric insulating annulus, see figure 2.14. The RRDE is used to study reaction intermediates, and determine what and how much is produced. The two electrodes are controlled independently of each other and can be set at different currents and potentials.

Collection efficiency

By using a RRDE the collection efficiency can be calculated. The disk will pass a constant current which generates a constant flow of intermediates or products. The ring is then set on a constant potential, and it is important to set the potential right so whatever was produced on the disk is oxidized on the ring. Some of the intermediates will not be oxidized on the ring, and escape into the bulk, so the ring current detected is only a fraction of the disk current. This fraction is called collection efficiency. See equation 2.22-2.25 for calculation of the theoretical collection efficiency.

Figure 2.14: A picture of a RRDE, [23].

The equations for calculation of the theoretical collection efficiency are [22]

$$N_0 = 1 - F\left(\frac{\alpha}{\beta}\right) + \beta^{\frac{2}{3}}[1 - F(\alpha)] - (1 - \alpha - \beta)^{\frac{2}{3}}\left\{1 - F\left[\left(\frac{\alpha}{\beta}\right)(1 + \alpha + \beta)\right]\right\} \quad (2.22)$$

Where N_0 is the collection efficiency, and α and β are constants dependent on the geometry of the RRDE

$$\alpha = \left(\frac{r_2}{r_1}\right)^3 - 1 \quad (2.23)$$

$$\beta = \left(\frac{r_3}{r_1}\right)^3 - \left(\frac{r_2}{r_1}\right)^3 \quad (2.24)$$

The RRDE dimensions are listed in appendix B.

The function F(θ) can be written as

$$F(\theta) = \left[\frac{3^{\frac{1}{2}}}{4\pi}\right] \ln\left[\left(\frac{1+\theta^{\frac{1}{3}}}{1-\theta}\right)\right] + \left[\frac{3}{2\pi}\right] \arctan\left[\frac{2\theta^{\frac{1}{3}}-1}{3^{\frac{1}{2}}}\right] + \frac{1}{4} \quad (2.25)$$

Values for θ is tabulated, [22].

To calculate the experimental collection efficiency, the ring current density is divided by the disk current density. [22] The two currents pass in opposite directions, hence the negative sign.

$$N_0 = -\frac{j_R}{j_D} \quad (2.26)$$

A RRDE with two rings is given here for demonstrative and comparison purpose. It would be similar to the ring-disk configuration in figure 2.14, but now with an additional ring outside the first ring, see figure 2.15.

Figure 2.15: A sketch of the hypothetical rotating ring-ring-disk electrode. The grey parts are insulating areas, and the white areas are the disk electrode and the two ring electrodes.

The collection efficiency on the second ring was calculated to be 17.2%. The dimensions were the same as for the RRDE in figure 2.14, and equations 2.22-2.25 were used. Here r_1 is still the same, but r_2 is the inner radius of the second ring, and r_3 is the outer radius of the second ring. The first ring is considered to be part of the insulating area in this calculation.

However, due to the complexity of manufacturing, and the usability of such an electrode assembly, it is not currently being used as other simpler designs that resemble the same features exist. The principle of comparison with the multielectrode microfluidic channel device.

2.6 Electrochemical Impedance Spectroscopy

All the component steps in an electrochemical process contribute to a total potential drop across the electrode-electrolyte interface, electrolyte resistance (R_S) and electron transfer resistance (R_{CT}), see figure 2.16.

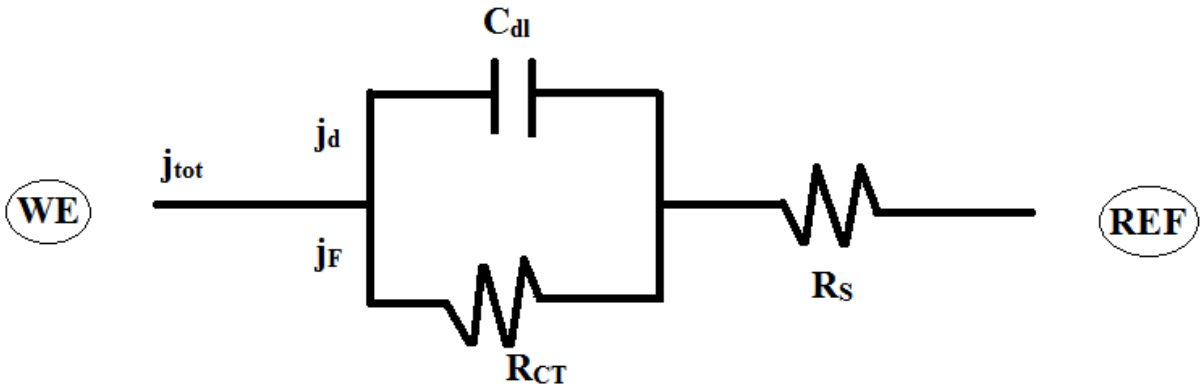

Figure 2.16: An example of the equivalent circuit between the working electrode and the reference electrode.

The total current in the cell is split into two currents, displacement current from the charging of the capacitor, and the faradic current from the electron transfer reactions, see equation 2.27

.

$$j_{tot} = j_d + j_F \tag{2.27}$$

In cyclic voltammetry the potential is varied between two limits, in electrochemical impedance spectroscopy the potential is held constant and a small amplitude sinusoidal wave is added on top of the DC signal. The frequency of the sine wave is varied and the amplitude of the wave is set to a constant value, typically 5 mV_rms.

When the frequency is high, the capacitance can't follow the perturbation and acts like a wire, Z_C approaches zero and the total impedance is equal to Z_{Rs}. At low frequencies the impedance of the capacitor becomes infinity and the overall impedance becomes a sum of the two resistances, R_S and R_{ct}.

$$Z_c = -\frac{i}{\omega c} \tag{2.28}$$

$$Z_{Rs} = R \tag{2.29}$$

In these equations i is the imaginary unit $\sqrt{-1}$, ω is equal to 2πf where f is the frequency, c is the capacitance, R is the resistance and Z_C and Z_{Rs} is the impedance component of the capacitor and resistance respectively.

The total impedance consists of an imaginary and real component, and a Nyquist plot images the imaginary impedance versus the real impedance of the cell, see figure 2.17 for an example. The electrolyte resistance R_S, is the value on the x-axis where the high frequency part of the curve intersects the real axis.

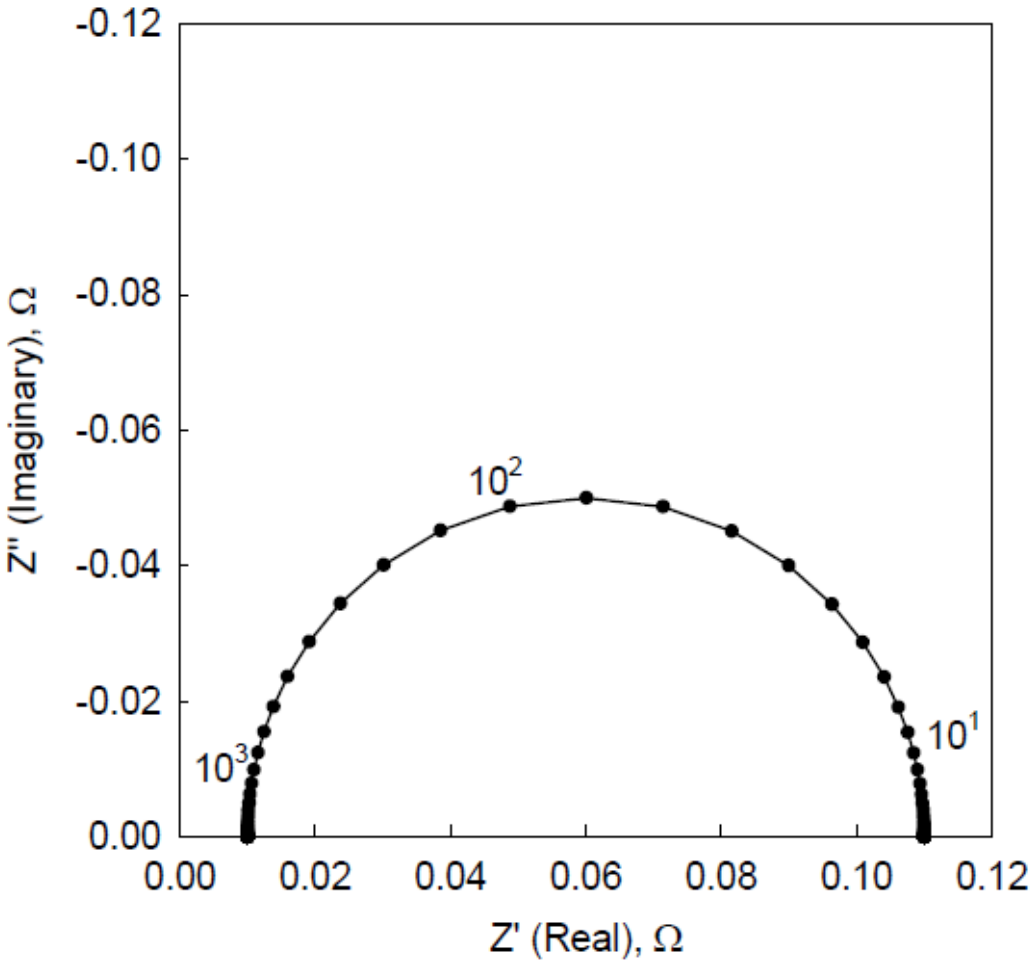

Figure 2.17: An example of a Nyquist plot, [24].

2.7 Photolithography

Photolithography is used to transfer a pattern from a mask to a photoresist on a substrate. This is done through several steps, [25], see figure 2.18 for flow sheet for the whole process.

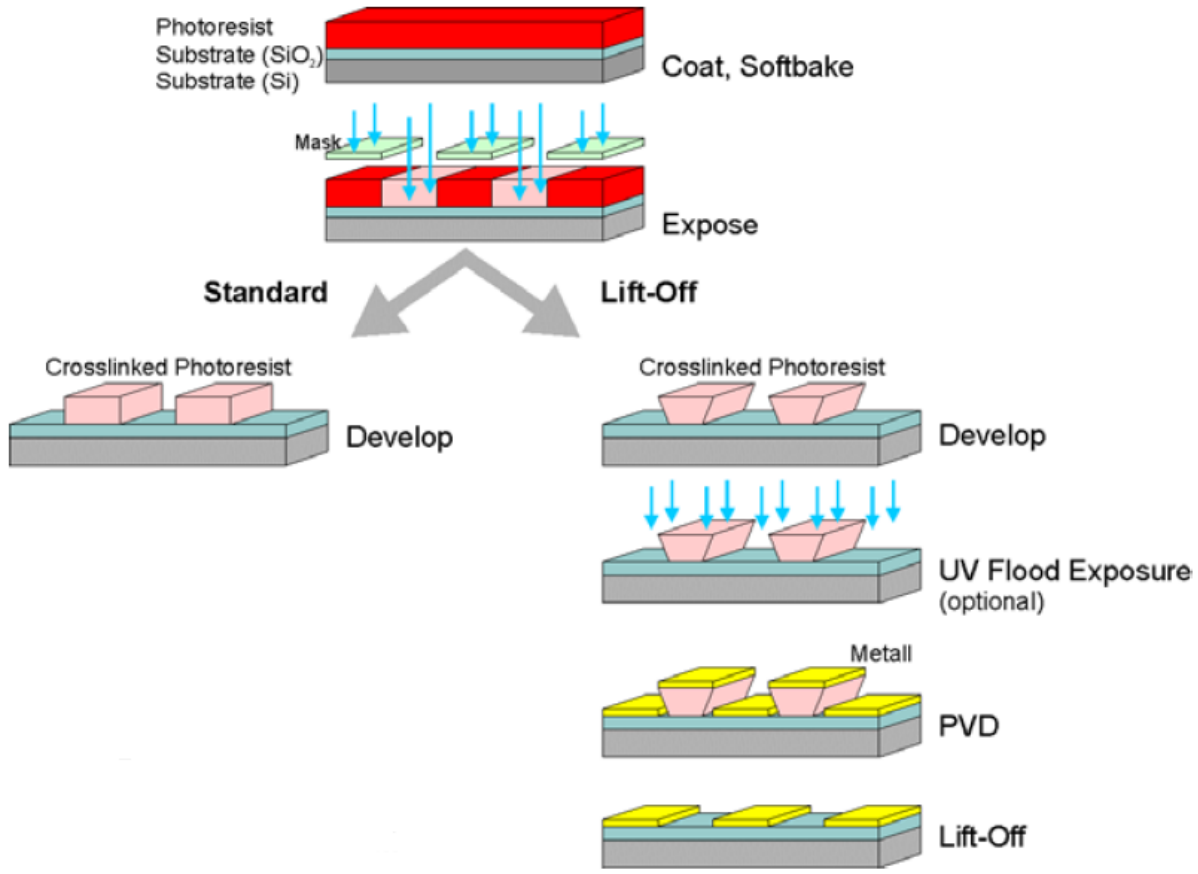

Figure 2.18: Flow sheet of the photolithography process, [26]. In this flow sheet a negative photoresist is used.

The photoresist is light-sensitive so it is important to do the following steps in an area with yellow light. First, the substrate is cleaned to remove any organic contaminant on the surface. To remove humidity and remaining organic solvents the substrate is heated on a hot plate for a few minutes. This is called dehydration bake. The application of the photoresist is done with a spin coater. A higher rotation speed gives a thinner photoresist film layer. The same spinning speed will give a different photoresist film layer thickness for the different types of photoresists with different viscosity. After spin coating the substrate is prebaked on a hot plate for a few minutes. The prebake time will be different for the different photoresists, and helps the photoresist polymer to cross-link during exposure. A negative photoresist polymer will start to cross-link with each other during UV-exposure.

During the UV exposure only parts of the photoresist is exposed to the UV-light because the pattern on the mask blocks the light, i.e. only parts of the photoresist polymer will start to cross-link. If the exposure is insufficient, the UV-light will not penetrate the photoresist film layer and the cross-linking is not initiated throughout the polymer. Too long exposure will cause exposure of UV-light to the area surrounding the pattern.

The photoresist is removed with a developer specific to the photoresist, which removes the uncross-linked photoresist. This makes it possible to deposit a metal layer in the desired pattern upon the photoresist. There is more than one way to deposit a metal layer, but only the electron beam evaporator is briefly explained here. The desired metal is heated until it evaporates, and deposits on the substrate. This metal layer will be very homogeneous and directional compared to electrodeposition.

The last step is lift-off where the substrate is immersed in a remover, which is specific for the different photoresists. The remover removes the rest of the photoresist (the cross-linked photoresist) with the metal layer on top, see figure 2.19 for an example after a successful lift-off.

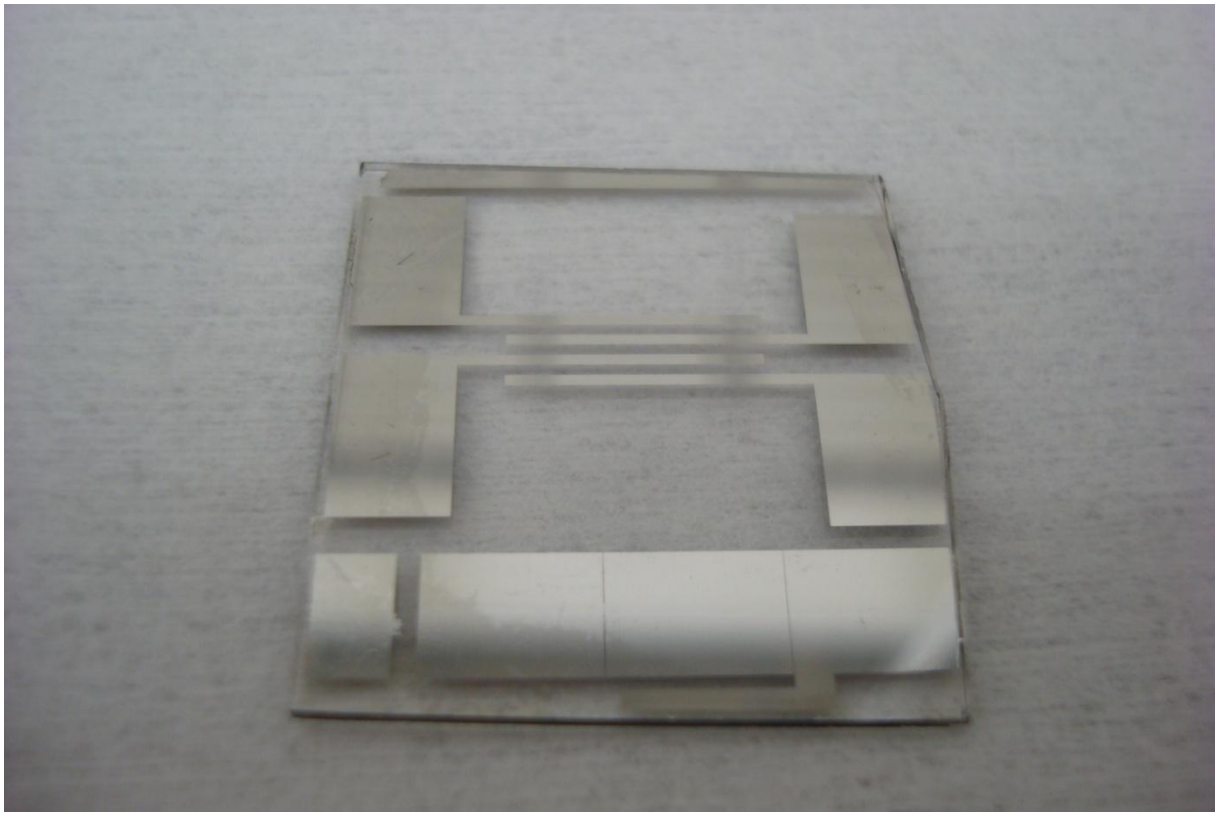

Figure 2.19: Glass chip with 500 µm wide platinum electrodes.

3 Literature study

3.1 Photolithography for fabricating MFFCs

Photolithography is a well established method for transferring a pattern from a photomask to a substrate, and well studied in literature [16], [9], [27], [28], [25], [29]. Also the fotoresist companies have their own guidelines in using their products, [26], [30], [31], [32]. The type of photoresist is determined by the substrate used, pattern to be transferred and its size and the use of the cell.

The photoresist layer thickness is a very important factor, and is decided by the type of photoresist (its viscosity), spinning rate and spinning time, [1]. If a thicker photoresist layer is desirable, it is possible to apply more than one layer of photoresist; apply, prebake, exposure, postbake on top of each other and a simultaneously development at the end, [27], [28], or apply one layer, prebake, apply another layer, prebake and so on and do a simultaneously exposure, postbake and development at the end. The first option requires that the mask is perfectly aligned over the same spot during every exposure, which can be difficult. The UV-exposure dose is probably easier to find with the first options since each layer will correspond to an exposure dose given by the manufacturer. Their guidelines are rough but not too far away from the optimal value. With the second option it might take some time to find the optimal UV-exposure dose, because even though the photoresist layer is doubled, it does not mean the UV-exposure dose has to be doubled.

As reported by Mata et al., [28], it is critical to remove all edge beads from the photoresist layer after spin coating, because this flaw will never go away if not removed immediately. This problem is particularly for photoresists with high viscosity, like the SU-8 2100. The development time increases with the number of photoresist layers, but it should have no effect on the feature quality.

Finding the right UV-exposure dose can be difficult, [25], and depends on the type of photoresist, the photoresist layer thickness and how old the lamp is. UV-exposure initiates cross-linking in the photoresist. An older lamp will need a longer exposure time than a younger lamp. A too high exposure dose causes the area surrounding the desired features on the mask to be exposed and creates “shadows”. In case of insufficient exposure, the UV-light is not able to penetrate the whole photoresist layer, and thus the cross-linking is not initiated throughout the layer. Depending on the photoresist, it should be post-exposure baked immediately after exposure to aid the cross-linking process.

If the UV- exposure is done correctly, the development step should go fine. During development the uncross-linked photoresist is removed. A negative photoresist will start to cross-link with each other during UV-exposure, which means that the unexposed areas will be removed during development, and the exposed area is removed with a positive photoresist, [33].

4 Experimental

4.1. Procedure for making a Micro fluidic flow cell

4.1.1 Making the electrodes on the glass chip.

The whole procedure of making the MFFCs took place in the nanolab clean room at NTNU, ISO 5+6, the cleanest area. Because a photoresist was used, everything was done in the photolithography area, an area with yellow light.

The glass chip (2.5 cm x 2.5 cm) was thoroughly cleaned with acetone (VWR International AS), isopropyl alcohol (VWR International AS) and dried with nitrogen gas (compressed nitrogen gas, AGA AS). To remove any organic contamination the glass chip was placed in a piranha solution. Piranha is a 3:1 mixture of concentrated sulphuric acid (95%, VWR International AS) and hydrogen peroxide (30 %, VWR International Ltd.). The glass chip was washed with deionized water, and dried with nitrogen gas. It is very important to remove any contaminants because it can have a huge effect on later steps. The next step was dehydration bake where the glass chip was placed on a hot plate at about 250°C for 5 minutes and cooled down.

Next step was spin coating where a negative photoresist is applied. The negative tone photoresist ma-N405 (micro resist technology GmbH) gives a film thickness of about 0.7- 0.8 µm at 1000 rpm for 30 s, and afterwards the glass chip was placed on a hot plate at 100 °C for 1 min. The negative tone photoresist ma-N440 (micro resist technology GmbH) gives a film thickness of about 2.5 µm at 1000 rpm for 30 s, and afterwards the glass chip was placed on a hot plate at 95 °C for 5 min. See Appendix C, and figure C.1 for the spin curves given by the manufacturer.

A mask with different mask patterns had previously been made. Each mask pattern represents different electrode dimension and the mask pattern with 50 µm, 100 µm and 500 µm electrode dimensions were chosen. The UV exposure (λ=365 nm) was done with a Maskaligner (model Karl Suss MA56) and the exposure time was 50 seconds for the ma-N405 photoresist and 226 s for the ma-N440 photoresist. The lamp had a constant intensity equal to 5.7 $mWcm^{-2}$. During the exposure it is possible that some of the UV- light goes through the glass chip and is reflected back which will ruin the photoresist layer. Therefore an UV-filter adhesive film (Solaronix) was placed under the glass chip during exposure, to prevent this from happening. After exposure the glass chip with the ma-N405 photoresist was immersed in a developer, ma-D331/s (micro resist technology GmbH), until all the photoresist was gone, about 2 minutes and 45 seconds. The glass chips with the ma-N440 photoresist were immersed in another developer, ma-D332/s (micro resist technology GmbH). The glass chip was examined in a microscope with yellow light to make sure that all the photoresist was gone and that the electrode pattern was still intact. It should be over developed so an undercut profile is obtained, see Appendix C, figure C.2.

When all the photoresist was removed and an undercut profile was reached, 10 nm titanium and 25 nm platinum was deposited on the glass chip, which was done with an electron beam evaporator (model Pfeiffer Vacuum Classic 500). To remove the metal outside the electrodes, the remover mr-Rem 660 (micro resist technology GmbH) was used, and assisted by an ultrasonic bath and a small brush.

4.1.2 Making the flow channel from PDMS and attaching wires.

The glass chip was cleaned and dried properly as explained earlier and a negative tone photoresist was applied with a spin coater (Spin150-NPP-IND). For the SU-8 2100 photoresist the glass chip was also cleaned with oxygen for a few minutes in a plasma cleaner (model Diener electronic, Femto) and then baked on a hot plate at 250 °C for 5 minutes. The Negative Tone Photoresist SU-8 5 gives a photoresist film thickness of about 12-15 µm at 1000 rpm for 30 seconds and SU-8 2100 gives a photoresist film thickness of about 100 µm at 3000 rpm (500 rpm/250 rpm s^{-1}/20 s and then 3000 rpm/250 rpm s^{-1}/40 s), see Appendix D, figure D.1 and D.2 for the spin curve for both photoresists given by the manufacturer. Especially for the SU-8 2100 it is very important to remove all edge beads before prebake. Before the SU-8 2100 photoresist was applied, a thin layer of SU-8 2 (3000 rpm, 30 seconds) was applied, to give strength to the SU-8 2100 photoresist layer. The SU-8 2 photoresist was soft baked, 1 minute at 65 °C and 2 minutes at 95 °C, flash exposed meaning the whole surface was UV-exposed but not developed, and at last post-exposure baked at 65 °C for 1 minute and at 95 °C for 2 minutes.

After spin coating the glass chip followed a 2-step softbake program, first at 65°C for 2 minutes and then at 95°C for 5 minutes on a hot plate for the SU-8 5 photoresist. For the SU-8 2100 photoresist the glass chip was placed on a hotplate at 65 °C for 5 minutes and then the hotplate was ramped up to 95 °C and it laid there for 20 minutes at 95 °C. Then the glass chip was placed on another hotplate at 65 °C for 2 minutes and cooled down to room temperature.

The same mask as used before had a channel pattern with a channel width of 1 mm. The UV exposure (λ=365 nm) was done with a Maskaligner (model Karl Suss MA56) and the exposure time was 26 seconds for the SU-8 5 photoresist and 54 seconds for the SU-8 2100 photoresist. The lamp had a constant intensity equal to 4.5 $mWcm^{-2}$. After exposure the glass chip followed a 2-step post exposure bake program, at 65°C for 1 minute and then at 95°C for 2 minutes on a hot plate for the SU-8 5 photoresist and 65 °C for 5 minutes, ramped up to 95 °C, stayed at 95 °C for 12 minutes and then the hot plate was turned off and the glass chip cooled down to room temperature on the hot palate (about 1 h) for the SU-8 2100 photoresist.

Then the glass chip was immersed in a developer, mr-Dev 600 (micro resist technology GmbH), until all the photoresist was gone, about 15 minutes for the SU-8 5 and 22 minutes for the SU-8 2100, and then rinsed in isopropyl alcohol (VWR International AS). If there are no white stripes when rinsed in isopropyl alcohol, the development should be done.

PDMS is very contaminating, and all work must be done in a specified hood for working with PDMS. About 25 g of Silicone elastomer base (Sylgard) and about 2 g of Silicone elastomer curing agent (Sylgard) was mixed thoroughly in a cup, and degassed in vacuum until all the bubbles were gone. Some of the PDMS were poured in a plastic dish, and the glass chip was placed with the channel up in the dish, and it was made sure that there was no air gap between the plastic dish and the glass chip. The rest of the PDMS was poured over the glass chip(s) and again degassed in vacuum until all the bubbles were gone, and then heated in an oven until the PDMS was hard, about 40 minutes at 80°C. The channel is then cut out with a scalpel, with the appropriate space around the channel, but not too much so that the area that connects the electrodes to the wires are covered, and inlet and outlet holes with the right size,1 mm, are made at each end of the flow channel. The glass chip and PDMS slab (channel up) are cleaned with air in a plasma cleaner (model Diener electronic, Femto) for 2 minutes. After plasma cleaning the PDMS slab (channel down) is placed on the glass chip right away, and heated in an oven for about 30 minutes at 80°C.

Wires are attached to the electrodes using a silver conductive epoxy (MG Chemicals). An equal amount of epoxy is mixed well together and applied to cover the wire. It is important to cover the whole wire without spilling silver epoxy between the electrode connection areas so that contact between the electrodes occurs.

4.1.3 Problems from specialization project fall of 2011

The main problem from the work done last fall (2011) with the Specialization project, [34], (TMT 4500 Materials Technology) was to find the right exposure dose for the photoresist ma-N 440. If the photoresist is over or under exposed it will not show until the development step, and that step could be seen as the problem. If the photoresist is exposed right there should be no problems during development.

This problem was solved by changing the photoresist to a photoresist that gives a much thinner layer, and the first exposures were done with the suggested exposure dose by the manufacturer. A slight reduction in exposure dose seemed to be right, and several exposures were done followed by a successful development step.

4.2 Testing of the MFFC

An external hydrogen reference electrode and platinum counter electrode was connected in a circuit with the MFFC. An analog bipotentiostat from Pine Instrument Company, model AFRDE5, or a Gamry Reference 600 potentiostat was used to produce a voltage and apply it to the cell. The potential was first swept down to the lower potential limit and then to the upper potential limit (in all experiments). To change the flow rate a syringe was filled with electrolyte and a pump (Pump 33 Harvard Apparatus) was used to press the syringe piston. The MFFC has four electrodes, so the possibility for an internal reference and counter electrode is present.

The experimental setup for testing the microfluidic flow cell is shown in figure 4.1. Number one in the picture is the analog bipotentiostat, number two is the syringe pump and number three is the microfluidic flow cell. Figure 4.2 shows how the MFFC is connected to an external reference and counter electrode. MFFCs with 50 µm and 500 µm electrodes were tested.

Figure 4.1: Experimental setup. The MFFC (3) is connected to a syringe pump (2) and an analog bipotentiostat (1).

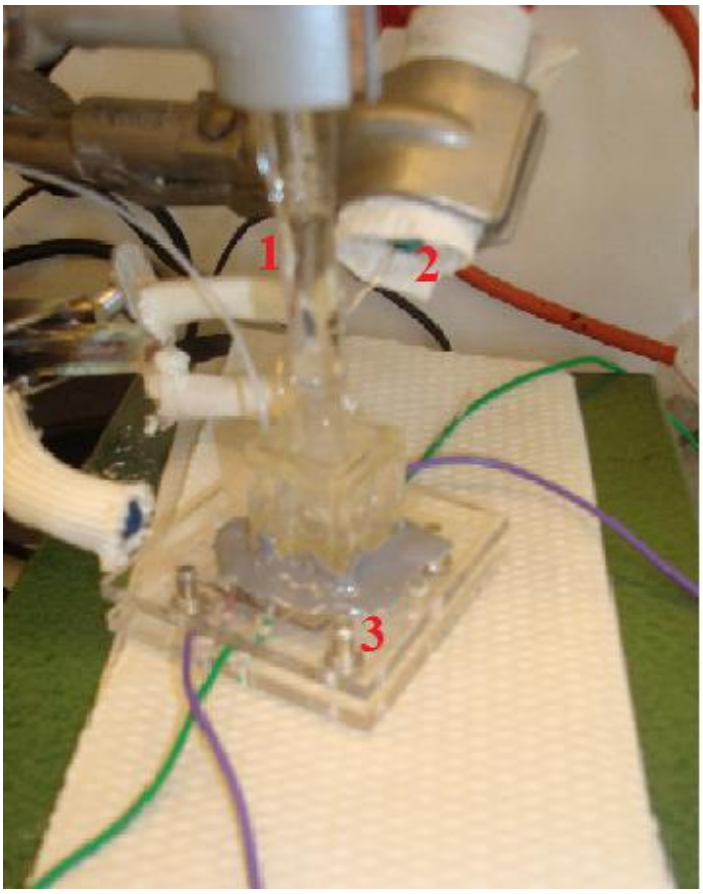

Figure 4.2: The MFFC (3) is connected to an external hydrogen reference electrode (1) and an external platinum counter electrode (2).

4.2.1 Cyclic voltammetry

Sulphuric acid

Constant flow rate, 0 µl min^{-1}, and different potential sweep rates, 10-500 mV s^{-1}. The electrolytes, 0.5 M sulphuric acid (H_2SO_4, 96 % sulphuric acid from Merck was diluted with ionized water) and 0.2 M potassium sulphate (K_2SO_4 from Alfa Aesar GmbH & Co KG, 99.0 %), was purged with argon gas (Yara Praxair AS). All four electrodes were used as working electrode, with external hydrogen reference electrode and platinum counter electrode.

The potential sweep rate was held constant at 100 mV s^{-1}, and different flow rates, 5-500 µl min^{-1}. The electrolyte, 0.5 M sulphuric acid (H_2SO_4, 96 % sulphuric acid from Merck was diluted with ionized water) was purged with argon gas (Yara Praxair AS) prior to the experiment. The first electrode was used as working electrode, the second as counter electrode and the fourth as reference electrode. The third electrode was not used in this experiment.

Ruthenium red-ox couple

Fresh 2.5 mM solution of the redox couple, hexaammineruthenium(II)chloride ($H_{17}Cl_2N_6Ru$, from Sigma-Aldrich) and hexaammineruthenium(III)chloride ($H_{18}Cl_3N_6Ru$, from Sigma-Aldrich) in 0.2 M potassium sulphate (K_2SO_4, from Alfa Aesar GmbH & Co KG, 99.0 %) was made fresh every day of testing. No flow rate, and potential sweep rate was varied from 10 mVs^{-1} to 500 mV s^{-1}. Constant potential sweep rate at 500 mV s^{-1} and the flow rate was varied from 1-500 µl min^{-1}.

4.2.2 Measurement of the electrolyte resistance in the MFFC

EIS

The MFFC (500 µm wide electrodes, 15 or 100 µm high flow channel) was connected in a circuit with a hydrogen reference electrode and a platinum counter electrode. Both the first and fourth electrode was used as working electrode. When internal electrodes were used as reference and counter electrode, the first electrode was reference electrode, the second was working electrode and the third was counter electrode.

Three potentials were used, 0.4 V, 1.0 V and 1.2 V. The frequency was between 0.1 Hz and 20 kHz, the amplitude was 5 mV rms, and 10 points per decade.

CV

Because of the high resistance in the cell the platinum oxide reduction peak will change with increasing sweep rate. This is an experimental evidence for high electrolyte resistance and can be estimated by assuming that the inverse of the polarization resistance equals the sloping part of the (quazi) steady-state polarization curve, [35], [36]. A linear regression curve is thus added to the cyclic voltammetry curve to calculate the electrolyte resistance, R_S.

4.3 Microfluidic fuel cell

4.3.1 Making the photomask for a microfluidic fuel cell

The electrode and channel design was chosen from Kjeang et al, [9], and drawn in AutoCAD. The electrode and channel design is similar to the example in figure 3.4. The electrodes are 500 m wide and separated by a 1000 µm gap. Two channel designs were made, one with a channel width if 2000 µm and one with a channel width of 2500 µm. The design allows two electrolyte streams to enter the cell and flow side by side down the channel.

5 Results

5.1 Microfluidic flow cells

5.1.1 Procedure for making the microfluidic flow cells

Ten glass chips with electrodes were made with the negative photoresist ma-N 405 where six had electrode dimensions of 50 µm, two had 100 µm electrode dimensions and two had 500 µm electrode dimensions, see figure 5.1 for a picture of a glass chip with 500 µm electrodes (1), electrode connections (2) and a flow channel with inlet and outlet (3). Titanium (10 nm) and platinum (25 nm) were deposited on the glass chips, and the lift-off process was completed in a couple of days. See Appendix E for pictures from each step in the procedure for making a microfluidic flow cell.

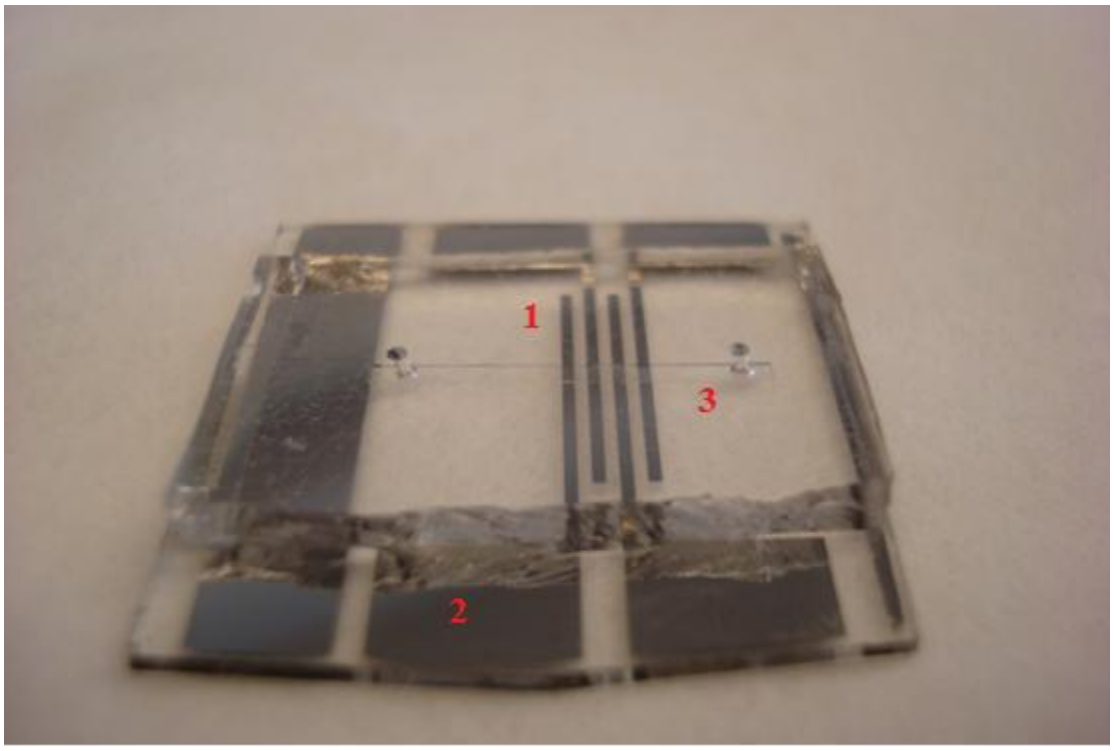

Figure 5.1: Glass chip with 500 µm wide platinum electrodes and PDMS slab, about 100 µm high flow channel.

Titanium (10 nm) and platinum (50 nm) were deposited on five glass chips with the ma-N405 photoresist. The development time was not long enough, about 52 seconds, so an undercut profile was not reached. After eight weeks the metal was still not removed, even with several hours in ultrasonic bath. The difference between the successful and unsuccessful lift-off processes was the development time and the amount of platinum deposited.

No microfluidic flow cells were made with the ma-N440 photoresist. The photoresist film layer was a lot thicker with this photoresist compared with ma-N405. Even though a UV-filter adhesive film was placed under the glass chip during exposure to hinder reflection of UV-light back on the glass chip, the photoresist still cracked during development. Both shorter

and longer exposure times than the suggested exposure time by the manufacturer was tried, without success.

The flow channel was made by making an impression in PDMS. The two photoresists SU-8 5 and SU-8 2100 gives a channel height of about 15 and 100 µm respectively. The procedure for SU-8 5 is much faster than SU-8 2100 but the photoresist layer thickness is much thinner. In this project a higher flow channel gave much better results, as seen in the results presented later.

The PDMS slab was attached to the glass chip by first activating the surface of both the PDMS slab (channel up) and the glass chip in a Plasma Cleaner, and then the PDMS slab was placed on the glass chip (channel down) and heated in an oven. Several times the PDMS slab did not stick properly to the glass chip, and the channel leaked during testing even though the screws were fastened tight. There was nothing to do but to try another glass chip and PDMS slab.

5.1.2 Cyclic voltammetry

The electrolyte was purged with argon prior to the experiment, but nevertheless some oxygen was dissolved in the electrolyte from when it was taken from the beaker with a syringe and to the microfluidic flow cell. This is seen in the voltammograms presented in later subchapters where the hydrogen area is lowered due to the dissolved oxygen in the electrolyte.

50 µm electrodes, 15 µm high flow channel

Cyclic voltammetry in both 0.5 M sulphuric acid and 2.5 mM ruthenium red-ox couple in 0.2 M potassium sulphate was tested with external reference and counter electrode. The results are presented in figures 5.2 and 5.3.

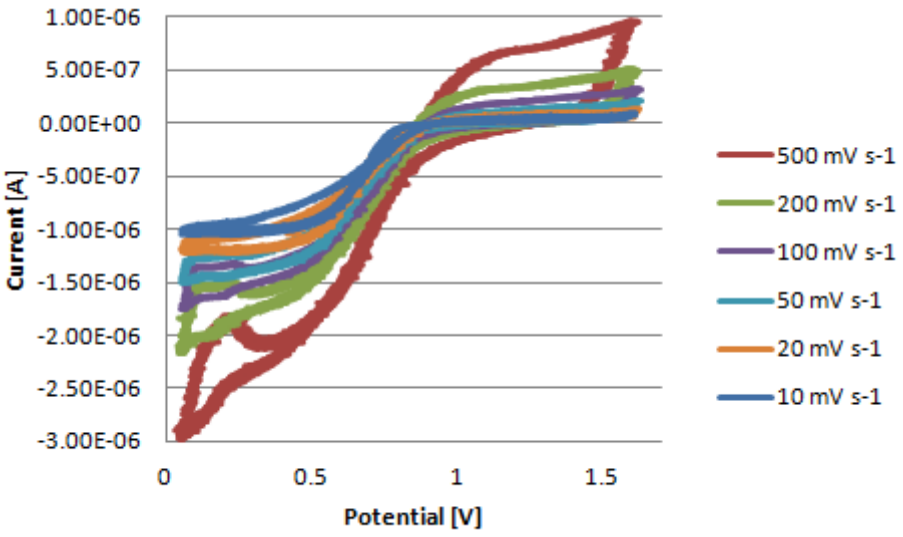

Figure 5.2: 0.5 M sulphuric acid, the third electrode is WE, external reference and counter electrode. No flow rate, potential sweep rate is varied, potential limits are 0.05 V and 1.6 V.

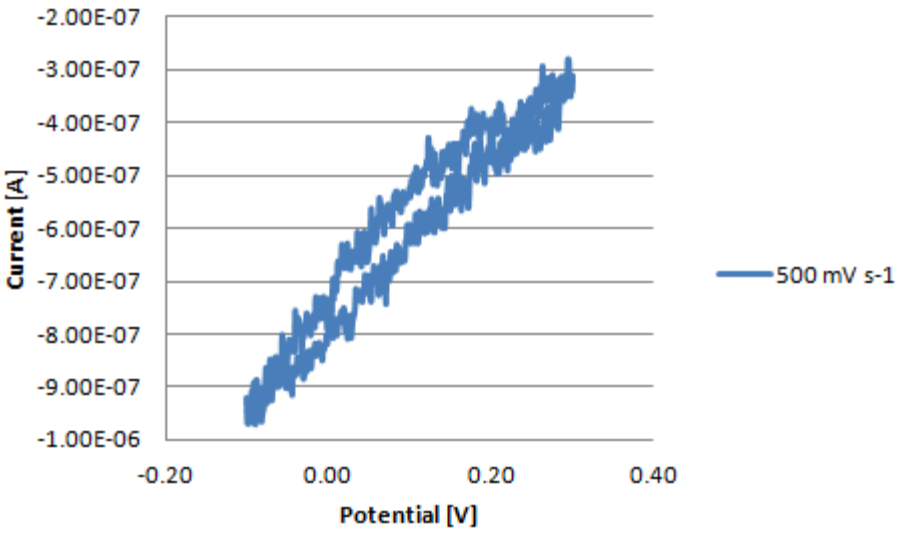

Figure 5.3: Ruthenium red-ox couple in K_2SO_4, the third electrode is WE, external reference and counter electrode. No flow rate, potential sweep rate is 500 mV s^{-1}, potential limits are -0.1 V and 0.3 V.

500 µm electrodes, 15 µm high flow channel

Cyclic voltammetry in both 0.5 M sulphuric acid and 2.5 mM ruthenium red-ox couple in 0.2 M potassium sulphate was tested with both external and internal reference and counter electrode. The results are presented in figures 5.4 - 5.8. As a mistake the working electrode and counter electrode switched places and was not discovered until the electrodes were changed

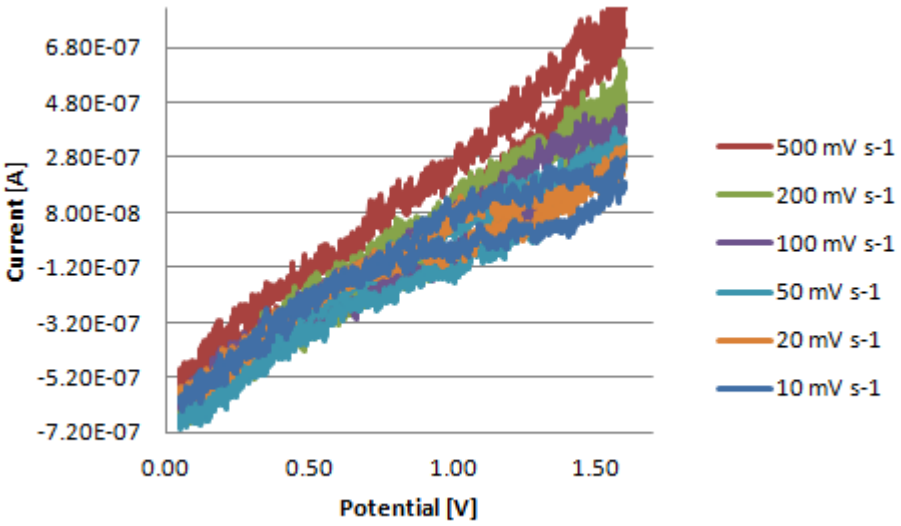

Figure 5.4: 0.5 M sulphuric acid, the third electrode is WE, external reference and counter electrode. No flow rate, potential sweep rate is varied, potential limits are 0.05 V and 1.6 V.

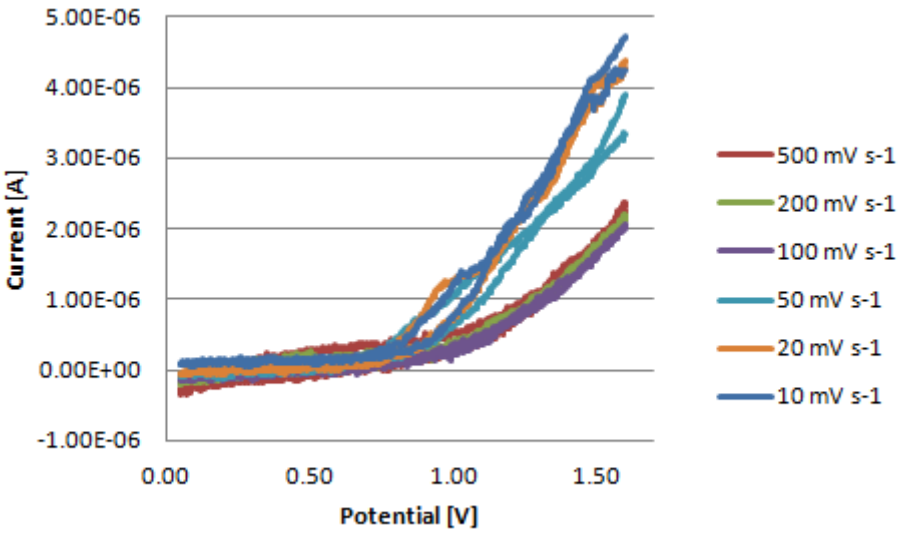

Figure 5.5: 0.5 M sulphuric acid, internal electrodes, E1-REF, E2-WE, E3-CE. No flow rate, potential sweep rate is varied, potential limits are 0.05 V and 1.6 V.

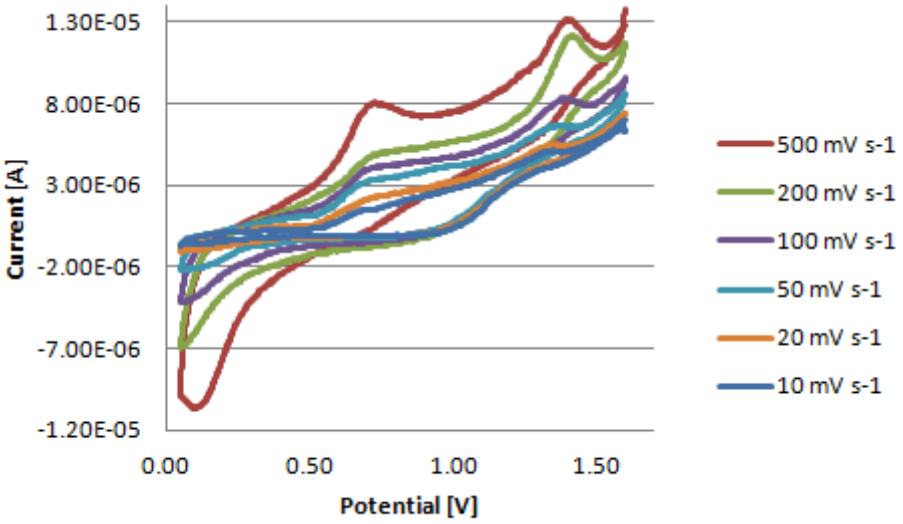

Figure 5.6: 0.5 M sulphuric acid, internal electrodes, E1-REF, E2-CE, E3-WE. No flow rate, potential sweep rate is varied, potential limits are 0.05 V and 1.6 V.

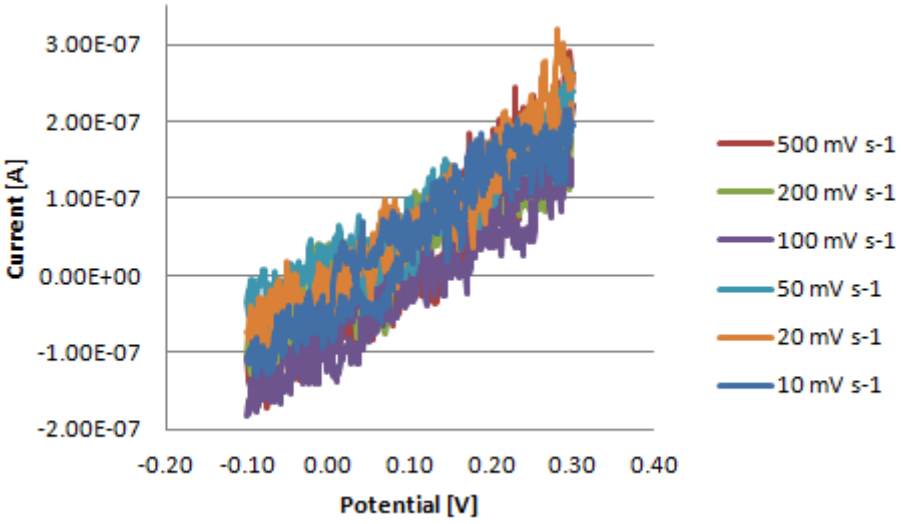

Figure 5.7: Ruthenium red-ox couple in K_2SO_4, internal electrodes, E1-REF, E2-WE, E3-CE. No flow rate, potential sweep rate is varied, potential limits are -0.1 V and 0.3 V.

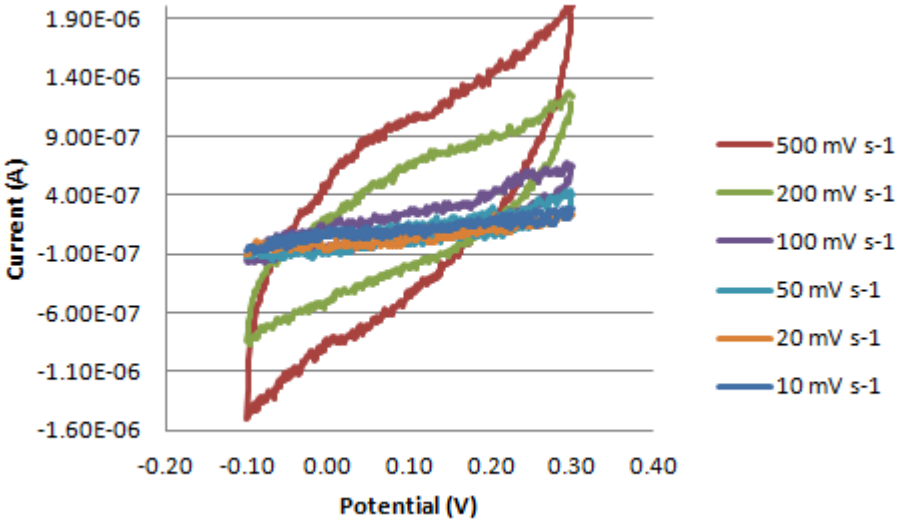

Figure 5.8: Ruthenium red-ox couple in K_2SO_4, internal electrodes, E1-REF, E2-CE, E3-WE. No flow rate, potential sweep rate is varied, potential limits are -0.1 V and 0.3 V.

500 µm electrodes, 100 µm high flow channel

Cyclic voltammetry in both 0.5 M sulphuric acid and 2.5 mM Ruthenium red-ox couple in 0.2 M K_2SO_4 was tested with external reference and external or internal counter electrode. The results are presented in figure 5.9 - 5.12.

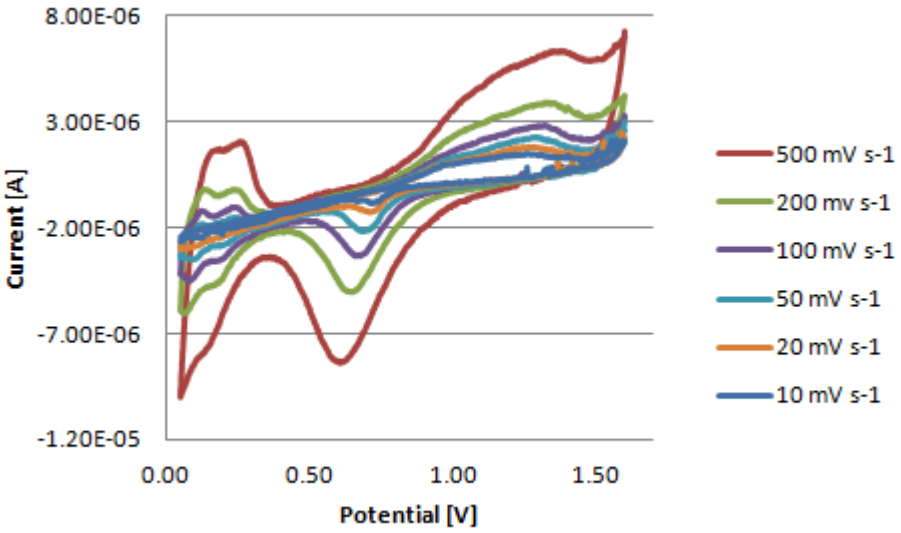

Figure 5.9: 0.5 M sulphuric acid, the third electrode is WE, external reference and counter electrode. No flow rate, potential sweep rate is varied, potential limits are 0.05 V and 1.6 V.

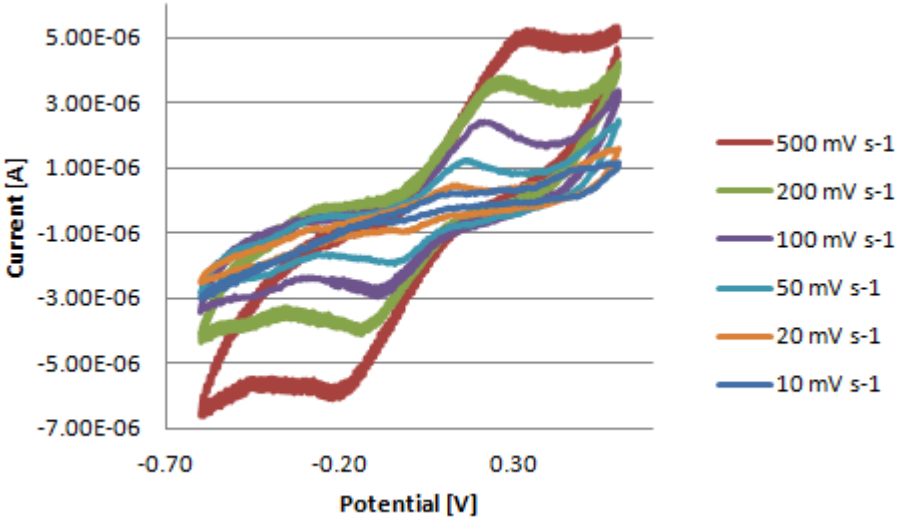

Figure 5.10: Ruthenium red-ox couple in K_2SO_4, the third electrode is WE, external reference and counter electrode. No flow rate, potential sweep rate is varied, potential limits are -0.6 V and 0.6 V.

The peak separation in figure 5. 10 varies from 133.8 mV to 534 mV, low to high potential sweep rate. At 50 mV s^{-1} the peak separation is 176.6 mV.

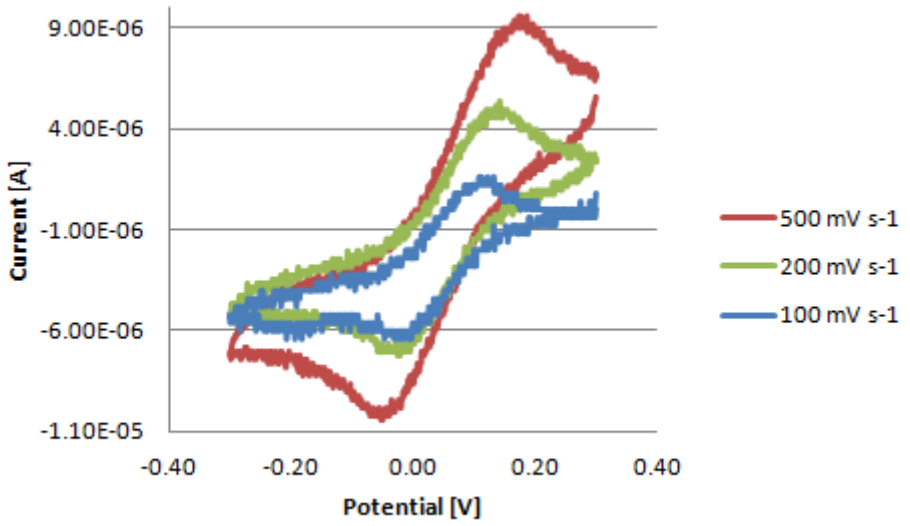

Figure 5.11: Ruthenium red-ox couple in K_2SO_4, the second electrode is WE, third electrode is counter electrode and external reference. No flow rate, potential sweep rate is varied, potential limits are -0.3 V and 0.3 V.

The peak separation in figure 5.11 varies from 137.6 mV to 227.2 mV, from low to high potential sweep rate.

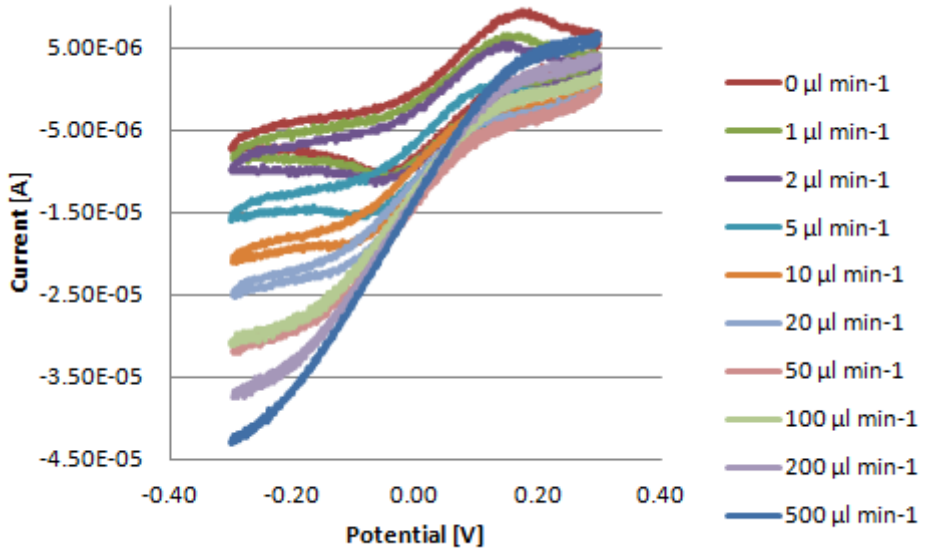

Figure 5.12: Ruthenium red-ox couple in K_2SO_4, the second electrode is WE, third electrode is counter electrode and external reference. A constant potential sweep rate at 500 mV s^{-1}, potential limits are -0.3 V and 0.3 V and the flow rate is varied.

The peak separation in figure 5.12 varies from 208.9 mV to 233.0 mV, from low to higher flow rate. The peak separation was only calculated for flow rates up to 10 µl min^{-1}.

The electrolyte was purged with argon, but not always for the same amount of time. The effect of argon purging is seen in figure 5.13, where the hydrogen region is much lower in one of the curves due to an increased amount of dissolved oxygen giving an increased overlying reduction current.

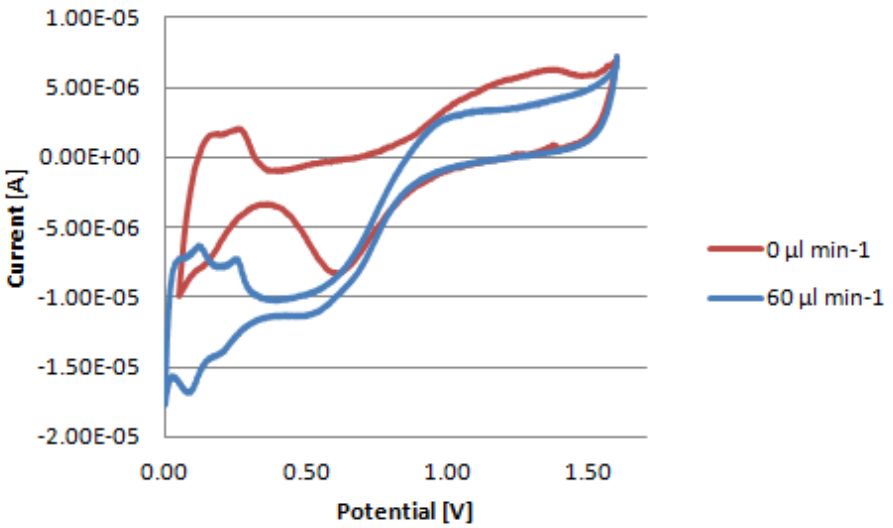

Figure 5.13: Cyclic voltammetry in 0.5 M sulphuric acid, 500 mV s^{-1}, top curve (red) was purged with argon gas and lower curve (blue) was not purged with argon gas.

External electrodes

Cyclic voltammetry with three external electrodes with 2.5 mM ruthenium red-ox couple in 0.2 M potassium sulphate was conducted in order to determine the potential limits for the MFFC later. The result is presented in figure 4.14. Here the lower potential limit is -0.1 V and the upper potential limit is 0.3 V. The peak separation for 500 mV s^{-1} in figure 5.14 is 68.8 mV and the peak separation decreases with decreasing potential sweep rate.

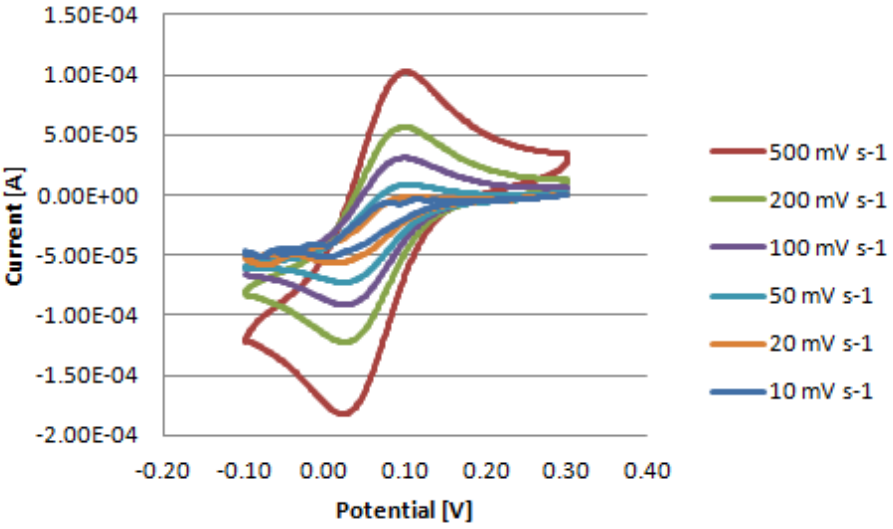

Figure 5.14: Cyclic voltammetry between -0.1 V and 0.3 V, no flow and the potential sweep rate was varied.

5.1.3 Measurement of the electrolyte resistance in the MFFC

The results from the cyclic voltammetry and the electrochemical impedance spectroscopy are presented in tables.

The electrolyte resistance from the electrochemical impedance spectroscopy was found by using the program ZsimpWin 3.22, which estimates a Nyquist plot to determine the electrolyte resistance. The results from both CV and EIS are presented further down in table 5.1 - 5.4.

500 µm electrodes, 15 µm high flow channel

The lower part of the negative going scan in the voltammograms, is presented with a trend line to give an approximation for the electrolyte resistance, figure 5.15 - 5.17.

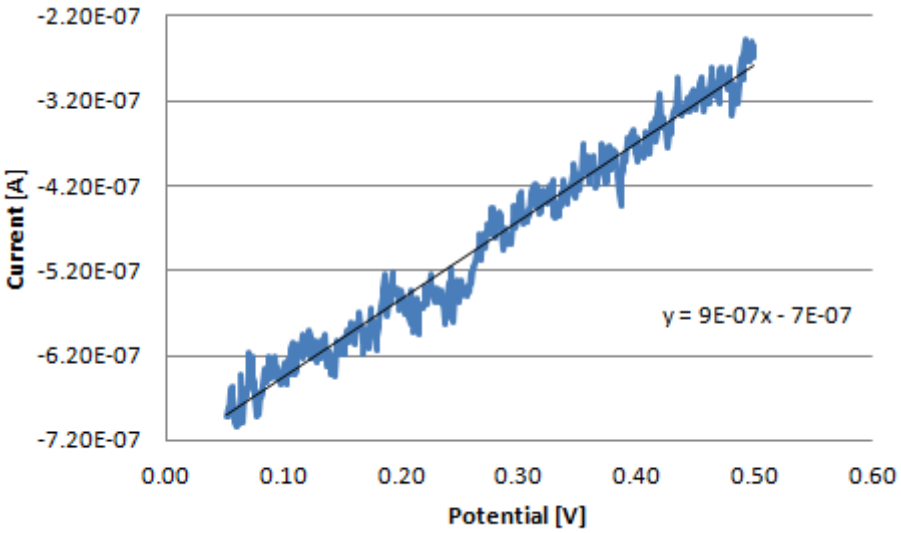

Figure 5.15: Cyclic voltammetry in 0.5 M H_2SO_4, E1-WE and external reference and counter electrode, potential sweep rate was 50 mV s^{-1}.

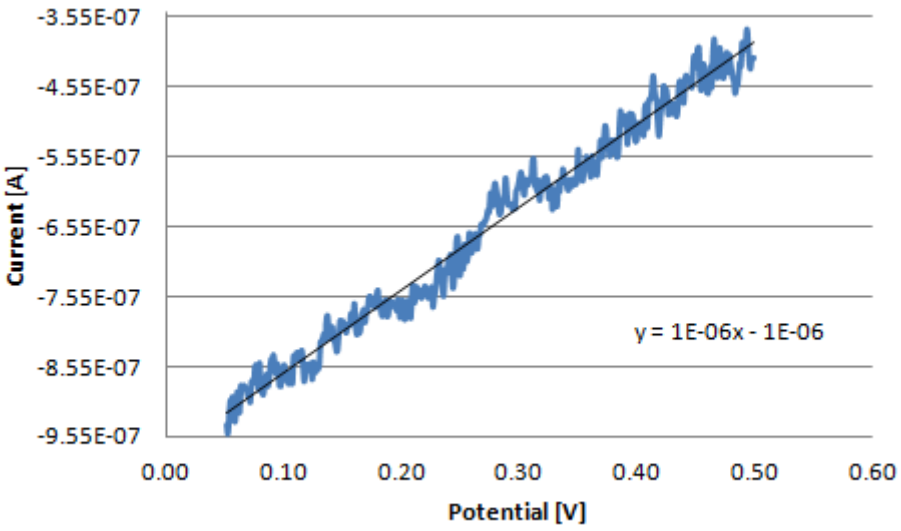

Figure 5.16: Cyclic voltammetry in 0.5 M H_2SO_4, E4-WE and external reference and counter electrode, potential sweep rate was 50 mV s^{-1}.

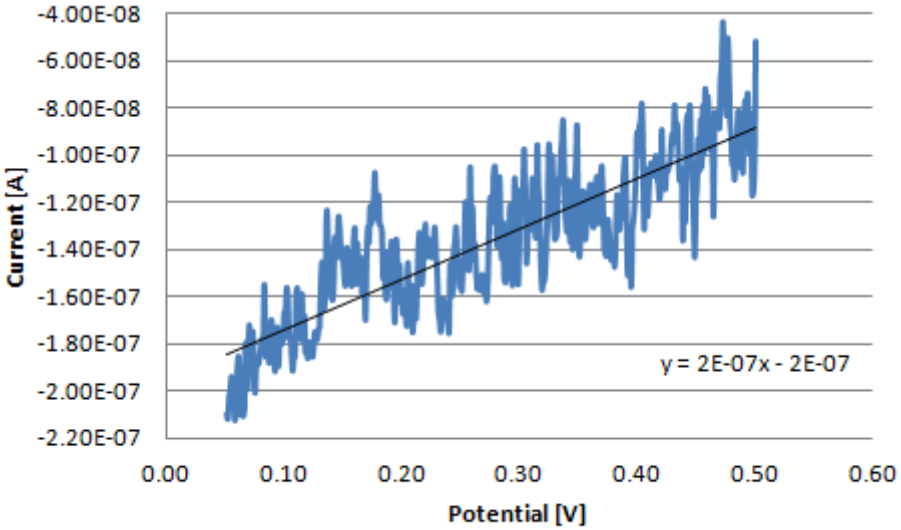

Figure 5.17: Cyclic voltammetry in 0.5 M H_2SO_4, E2-WE and internal reference and counter electrode, potential sweep rate was 50 mV s^{-1}.

In table 5.1 the results from both cyclic voltammetry with linear regression and electrochemical impedance spectroscopy are presented.

Table 5.1 Electrolyte resistance, R_S, calculated by CV with linear regression and EIS.

	CV	EIS, E = 0.4 V	EIS, E = 1.0 V	EIS, E = 1.2 V
E1 - WE (ext. REF and CE.)	1.11 M Ω	0.8442 MΩ	0.8638 MΩ	79.75 MΩ
E4 - WE (ext. REF and CE.)	1.00 MΩ	0.44 MΩ	0.6023 MΩ	0.566 MΩ
E1 - REF, E2 - WE, E3 - CE	5.00 MΩ	0.08915 MΩ	0.08244 MΩ	0.0785 MΩ

The lower part of the negative going scan in the voltammograms is presented with a trend line to give the electrolyte resistance, figure 5.19 - 5.21. Only the hydrogen area is included because the rest of the voltammogram is not linear, se figure 4.18.

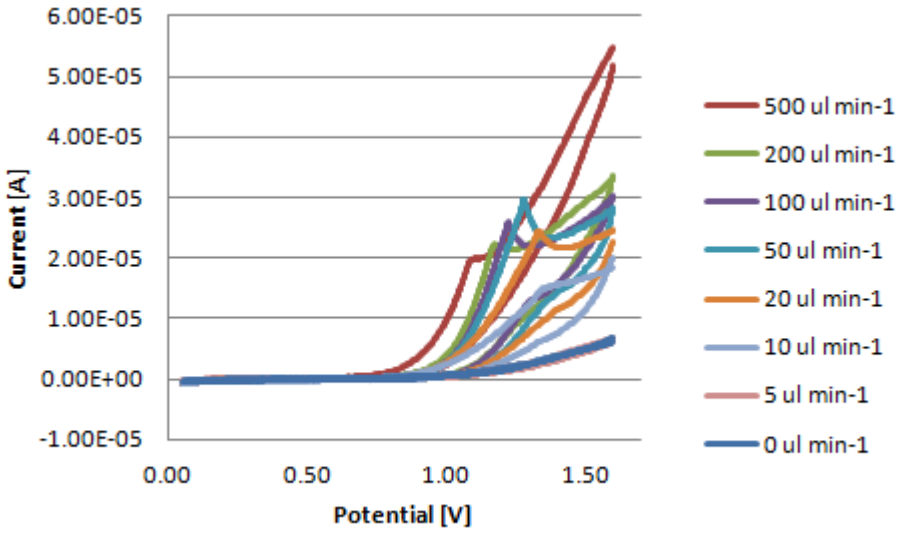

Figure 5.18: Cyclic voltammetry in 0.5 M H_2SO_4, E1-WE, E2-CE, E4-REF, potential sweep rate at 100 mVs^{-1} and the flow rate was varied from 0 to 500 µl min^{-1}.

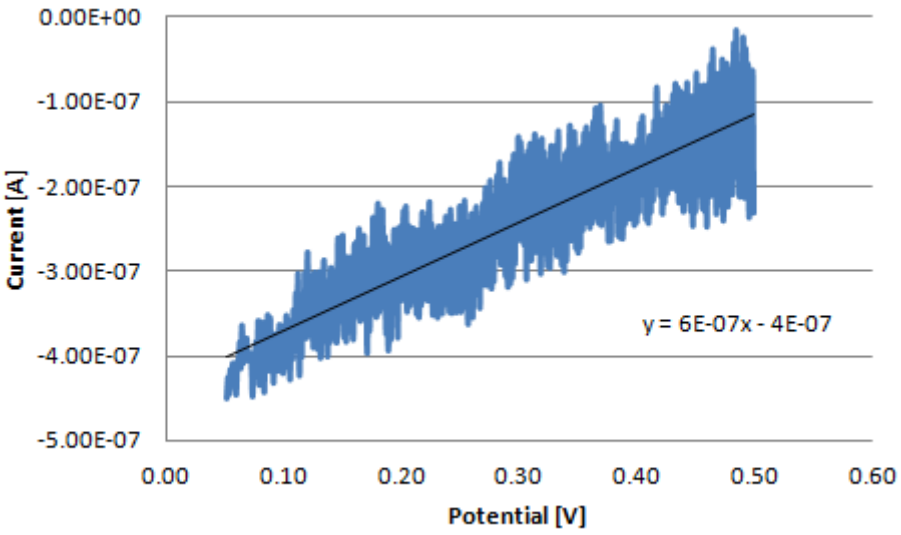

Figure 5.19: Cyclic voltammetry in 0.5 M H_2SO_4, E1-WE, E2-CE, E4-REF, potential sweep rate at 100 mVs^{-1} and no flow, 0 µl min^{-1}.

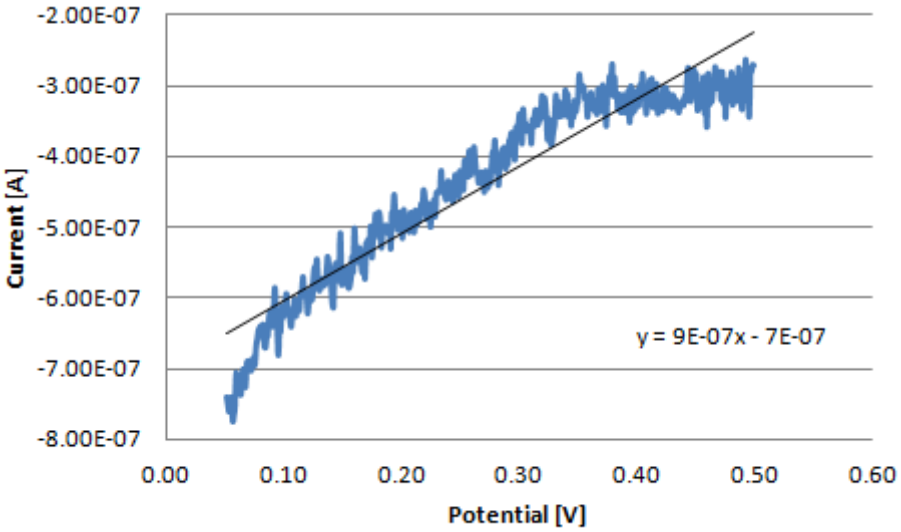

Figure 5.20: Cyclic voltammetry in 0.5 M H_2SO_4, E1-WE, E2-CE, E4-REF, potential sweep rate at 100 mVs^{-1} and a flow rate 10 µl min^{-1}.

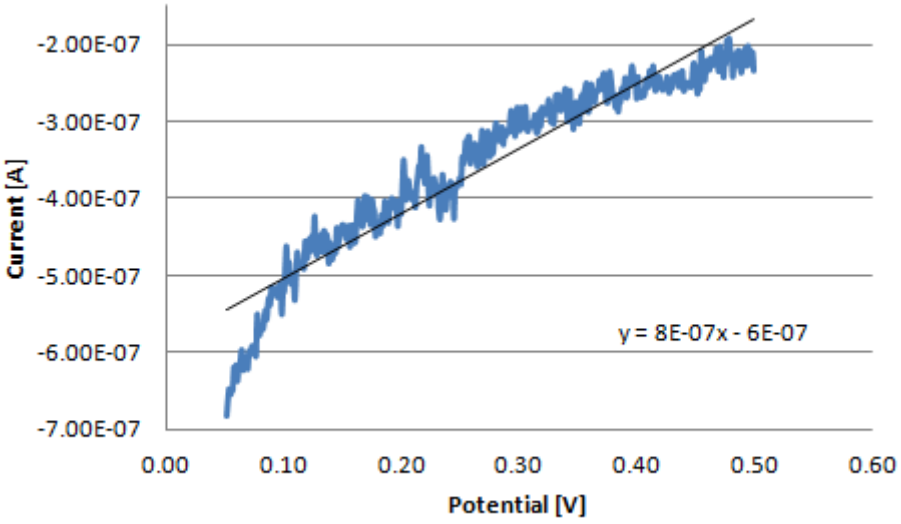

Figure 5.21: Cyclic voltammetry in 0.5 M H_2SO_4, E1-WE, E2-CE, E4-REF, potential sweep rate at 100 mVs^{-1} and a flow rate 100 µl min^{-1}.

In table 5.2 the results from both cyclic voltammetry with linear regression and electrochemical impedance spectroscopy are presented. The electrolyte resistance calculated from the linear region in the voltammograms is much higher than the electrolyte resistance calculated from EIS.

Table 5.2 Electrolyte resistance calculated from EIS for different potentials and flow rates.

	CV	E = 0.4 V	E = 1.0 V	E = 1.2 V
0 µl min^{-1}	1.667 MΩ	2.208 kΩ	0.3444 kΩ	0.5427 kΩ
10 µl min^{-1}	1.111 MΩ	3.249 kΩ	4.487 kΩ	0.3555 kΩ
100 µl min^{-1}	1.250 MΩ	18.04 kΩ	0.3336 kΩ	0.3642 kΩ

500 µm electrodes, 100 µm high flow channel

The results from the electrochemical impedance spectroscopy are not compared with the result from cyclic voltammetry for this cell, because the negative going scan of the voltammograms are no longer linear and the electrolyte resistance is low enough so the current signal can be detected. The results from the EIS are presented in table 5.3 and 5.4.

Table 5.3 Electrolyte resistance, R_S, calculated from EIS.

	EIS, E = 0.4 V	EIS, E = 1.0 V	EIS, E = 1.2 V
E1 - WE (ext. REF and CE.)	9745 Ω	9830 Ω	9598 Ω
E4 - WE (ext. REF and CE)	6225 Ω	6242 Ω	6059 Ω
E1 - REF, E2 - WE, E3 - CE	286.5 Ω	276.7 Ω	269,9 Ω

Table 5.4 Electrolyte resistance, RS, calculated from EIS, external hydrogen reference electrode and internal WE (E2) and CE (E3).

	EIS, E = 0.4 V	EIS, E = 1.0 V	EIS, E = 1.2 V
0 µl min^{-1}	6143 Ω	8360 Ω	6480 Ω
10 µl min^{-1}	7925 Ω	11.98 kΩ	26.68 kΩ
100 µl min^{-1}	5449 Ω	6853 Ω	5429 Ω

In figure 5.22 one of the electrochemical impedance spectroscopy results is presented. The Nyquist plot is generated by the program ZsimpWin 3.22. The red dots are the results, and the green dots are the Nyquist plot estimated by the program.

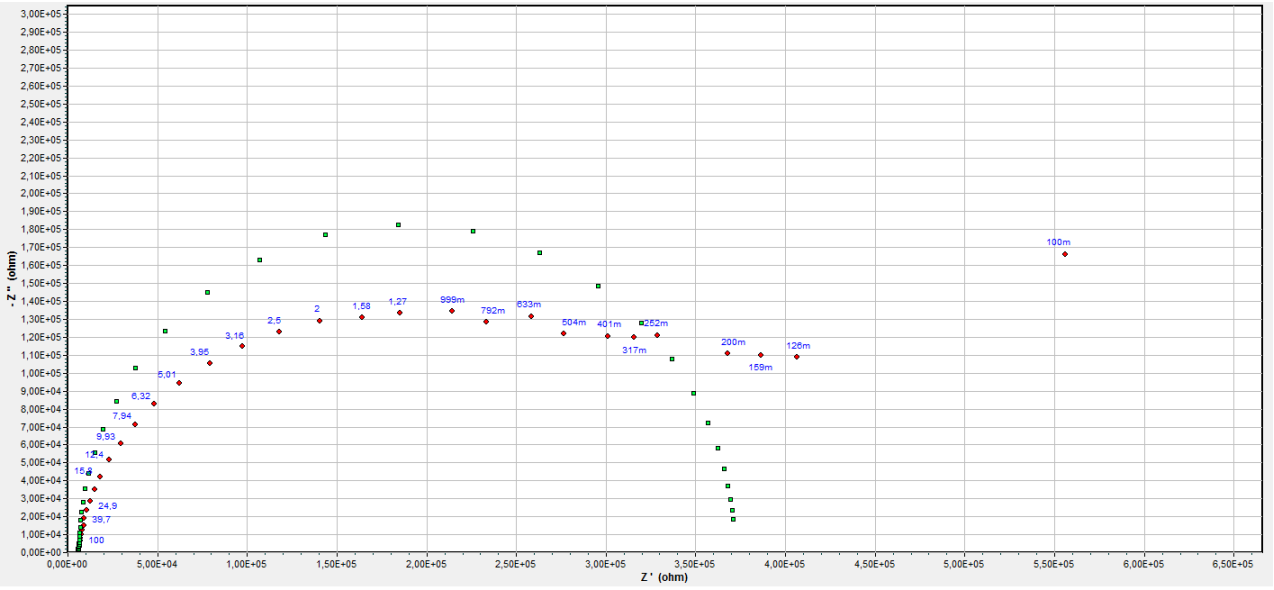

Figure 5.22: Electrochemical impedance spectroscopy results, external reference and counter electrode, E4-WE, E = 0.4 V, 0.1 Hz - 20 kHz, amplitude of 5 mV. Here, the electrolyte resistance is 6225 Ω.

5.2 Microfluidic fuel cell

5.2.1 Making the photomask for a microfluidic fuel cell

A new photomask with electrode and channel configuration for the UV-exposure in the photolithography routine was made. The microfluidic fuel cell design is shown in figure 3.4 and the chosen design was taken from Kjeang et al, [9]. The electrode and channel design was drawn in AutoCAD and a mask was made.

The electrode design consists of two electrodes which are 500 µm wide, with a separation of 1.0 mm. The mask has two channel designs, both are T-shaped, one where the channel is 2.0 mm wide and one where the channel is 2.5 mm wide. In both channel designs the channel is 11.5 mm long which gives an active electrode length of about 10 mm.

6 Discussion

6.1 Microfluidic flow cell

6.1.1 Procedure for making the microfluidic flow cells

In the procedure for making a microfluidic flow cell it was especially the undercut profile in the photoresist after development that made the difference. The process sheet provided by the manufacturer, [26], strongly advice to use undercut profile when depositing metal. Right away it was possible to see the photoresist coming off, compared to the glass chips without undercut profile where it took a while before any photoresist came off at all. By looking at the glass chip it is hard or impossible to see any difference between undercut profile and no undercut profile, but if the development time is increased significantly, an undercut profile should be reached. The manufacturer also advices to increase the prebake temperature, therefore the temperature was increased from 95 to 100 °C compared to the work done last semester in the specialization project (TMT 4500 Materials Technology), [34].

A very high temperature is required in order to evaporate platinum. The photoresist is temperature sensitive, and the high evaporating temperatures employed can damage the photoresist. Thus, the platinum deposition should be completed as fast as possible. Therefore the amount of platinum deposited was reduced by half, from 50 nm to 25 nm. It is hard to say if it would have worked with 50 nm platinum instead of 25 nm, but several co-workers in the nanolab have had trouble with the photoresist being destroyed by the high temperatures during platinum deposition. The reduction of the platinum layer may have helped, but the most important difference was the undercut profile in the photoresist layer.

Photolithography is a time consuming and delicate procedure and therefore every step in the whole routine can ruin the outcome of the various steps. During the UV-exposure it is important to use the right dose, if not, the photoresist could be under- or over-exposed. This error will not show until the development step, and it might be easier to find the right exposure dose when the photoresist layer is thinner. A UV-adhesive film was not enough with the ma-N440 photoresist, maybe if HMDS was used it could work. HMDS is evaporated on the substrate before the photoresist is spin coated on top, and is supposed to strengthen the photoresist.

PDMS does not form a strong and permanent bond to the glass chip, [25], not even after a couple minutes in the plasma cleaner which is supposed to activate the surfaces to increase the strength of the bond between the surfaces. One time a beaker was placed on top of the PDMS slab (during heating in the oven after plasma cleaning) to aid the bonding between the PDMS slab and the glass chip. Unfortunately it did not help, the beaker seemed to form a weak bond with the beaker even though it should not (only forms bond between two activated surfaces) and the bond between the PDMS slab and the glass chip may have been damaged when the beaker was removed. In later attempts to attach the PDMS slab no beaker was placed on top. Instead, the PDMS was pressed down on the glass chip, not over the channel, but around. This seemed to work better than the beaker on top.

Since the flow channel was not high enough it was necessary to increase the photoresist layer thickness by applying more than one layer of the photoresist SU-8 5 or try another photoresist which gives a thicker photoresist layer with only one application, like SU-8 2100. The problems with applying more than one layer are: (i) the information given by the manufacturer gives no indication of the exposure dose. Even though the photoresist layer thickness is doubled the exposure dose is not necessary doubled. Figuring out this procedure would take time, time that was not available towards the end of this project, (ii) applying one layer and then expose and develop and then apply a second and third layer and so on require that the mask is aligned with high precision over the same spot every time, [28]. This requires a good microscope, which the Maskaligner available in the Nanolab did not have. A new Maskaligner will soon be available to all Nanolab users with improved positioning features.

The SU-8 2100 photoresist is a difficult photoresist to work with because the viscosity is very high, so it makes it hard to handle. In this case, the pattern (channel pattern) was quite large and the channel structure did not need to be perfect, only close to 100 µm. Since the requirements were not that strict, completely straight walls inside the channel were not necessary, it was easier to make a channel. When a channel for a microfluidic fuel cell is to be made, the walls need to be straight otherwise the laminar flow will be disrupted, it might be harder to make a perfect channel. The exposure time of 54 seconds worked under these conditions and requirements, but it may not be the optimal exposure time for this photoresist with this layer thickness. Only one flow channel with this height was made, and no other attempts were made. This has to be pursued in the future.

6.1.2 Electrochemical measurement in MFFC

Cyclic voltammetry with external electrodes (WE, CE, REF) in 2.5 mM ruthenium red-ox couple in 0.2 M potassium sulphate electrolyte was performed in order to give the potential limits for later testing of the ruthenium red-ox couple in the MFFC. The results presented in figure 5.14 are similar to the results presented by Kjeang et al., [16] where the peak separation is 59 mV at 50 mV s^{-1} and in figure 5.14 the peak separation is 61.0 mV at 50 mV s^{-1}. The curve shape is alike and the reduction and oxidation peaks are almost at the same potentials (after correcting the potentials to the same reference electrode as the results presented by Kjeang et al. are with a silver/silver chloride reference electrode).

Effect of Dissolved Oxygen

The microfluidic flow cell is not a closed system, therefore there will be some oxygen present. When the concentration of oxygen increases in the electrolyte, the current response in the lower potential region of the voltammogram is gradually shifted to more negative currents, see figure 5.13. This is because oxygen reduction is diffusion controlled, and adds a constant, negative contribution to the current. Figure 3.8 shows a voltammogram where the electrolyte is purged with argon gas both before and during the experiments, and therefore not allowing any oxygen to dissolve. Argon purging during the experiment is not possible with a MFFC as it is in a multi-necked bottle, and must be done prior to the experiment. But there is a clear

distinction between no argon purging at all and argon purging before the experiment as shown by figure 5.13.

One solution could be to use a "glove box", [16], which is completely closed, and the atmosphere in the box would be oxygen free. Whether or not this would be practical is another matter.

Electrode placements

External or internal counter electrode had little or no significance, maybe because only small currents are transported between active platinum electrodes in a highly ionic solution (although solution resistance i quite high due to the narrow channel). When the counter electrode is placed internally, the reaction taking place on the electrode will have no effect on the current signal from the working electrode, as the counter electrode is placed down-stream of the working electrode. Positioning of the working electrode was less critical is seemed. However, the true problem aroused with the positioning of the reference electrode.

Effect of Channel Height

When the PDMS slab was properly attached to the glass chip with the electrodes and there was no leakage from the flow channel, and the wires were properly attached to each electrode, there still was something not working as intended. A multimeter was used to measure the resistance and connection between the electrodes and between the electrode and the wire. There was no connection between the electrodes and there was a connection between the electrodes and the wires. Since there was nothing wrong with the electrodes, the problem had to be the channel height. The electrolyte resistance was found to be very high, and therefore none of the experiments gave the expected results. All that was seen from the cyclic voltammogram was the presence of a resistance of great significance. This was because the flow channel was not high enough, the first cells that were made had a channel height of only15 µm. Therefore a higher channel was tried.

When the channel height was increased from 15 to 100 µm, the electrolyte resistance was significantly reduced and a considerable improvement of the shape of the cyclic voltammograms was seen in figures 5.9 - 5.12. All regions that are expected in a cyclic voltammogram for platinum electrodes in sulphuric acid are present, hydrogen region, double layer region and oxide region. The problem with oxygen being present was still there. All electrolytes were purged with argon gas prior to all experiments, but when the electrolyte was transferred from the beaker to the syringe and eventually the MFFC, some oxygen was dissolved in the electrolyte.

Effect of Electrolyte Flow Rate

In stationary systems the Nernst diffusion layer thickness is constant, meaning the concentration gradient increases with increasing potential, which in turn allows the current to increase, until the electrode surface concentration is zero. Then the current flattens, and will no longer increase with increasing potential, which could explain the high flow rate curves in figure 5.12. In systems with rotation or flow the Nernst diffusion layer thickness will decrease with increasing rotation or flow rate and a higher current is expected, [16]. However, it seems that the dissolved oxygen in the electrolyte has an impact on the current, especially at high flow rates. At low flow rates there is only a small change in the voltammograms, and the oxidation and reduction peaks are around the same potential values. But as the flow rate increases the cathodic current increases while the anodic current does not. At higher potential sweep rates the presence of oxygen is more dominating than at low potential sweep rates, and the results presented in figure 5.12 is at 500 mV s^{-1}, a high potential sweep rate. During testing there was a lot of noise in the current signal, and the results are not presented.

6.1.3 Measurement of the electrolyte resistance in the MFFC

The electrochemical impedance spectroscopy measurements confirmed that there was a significant electrolyte resistance present in the MFFC (500 µm electrodes, 15 µm high flow channel) and was calculated to be 0.4 - 1 MΩ which is very high. Normally an electrolyte resistance in the area of 1000 Ω is accepted. This high electrolyte resistance explains the lack of results from previous testing of cyclic voltammetry in sulphuric acid. The solution was to use a higher channel as seen from the results. The electrolyte resistance calculated from EIS for the MFFC with 500 µm electrodes and 100 µm high flow channel was 300 - 10000 Ω, much lower than the electrolyte resistance in the other MFFC.

Another possible way to reduce the electrolyte resistance could be to make a larger outlet hole. The problem is to know which hole is going to be outlet/inlet hole when the holes are made. When the cell is put together and the two plates are screwed together, often what was thought of to be inlet hole ends up being outlet hole. Therefore both inlet and outlet hole has been of the same size in this project.

6.2 Microfluidic fuel cell

6.2.1 Making the photomask for a microfluidic fuel cell

The reason to why two electrode designs were made is because in the first design the channel width is equal to the width of the two electrodes and the electrode separation. That means that the channel needs to be placed carefully on over the electrodes so they are both completely inside the channel. This is hard, and it is very likely that parts of one of the electrodes are outside the channel. In the second electrode design there is a little bit to go on so it is easier to place the channel over the electrodes with both electrodes completely inside the channel.

The flow channel is T-shaped, which means that anodic and cathodic stream is feed from each side, and they flow together down the channel. This channel design was chosen because it was used by Kjeang et al, [9], and it is a simple channel design for two electrolytes.

7 Conclusions

A routine for making a Microfluidic Flow Cell was established for the negative tone photoresist ma-N 405, and ten glass chips with platinum electrodes were made. For this project, the solution was to change to another photoresist, from ma-N 440 to ma-N 405, which gives a much thinner photoresist layer, use an UV-adhesive film under the glass chip during UV-exposure and a longer development time which gives the photoresist an undercut profile which helps during metal lift-off.

Metal (titanium and platinum) was vapour deposited on another five glass chips, also with ma-N 405, but it never came off completely. Most likely the development time was not long enough to secure an undercut profile in the photoresist layer. Also a thicker layer of platinum was vapour deposited, which could have affected the photoresist. A photoresist is very temperature sensitive, and platinum evaporates at a very high temperature which may destroy the photoresist.

The channel height is a very important factor. If the channel height is too low, the electrolyte resistance increases dramatically and the current signal gives no meaning. The first cells had a channel height of about 15 µm which was too low, seen from the voltammograms presented which indicates there is a significant resistance present. The electrolyte resistance was calculated from electrochemical impedance spectroscopy to be in the area of 0.4 - 1 MΩ, and was compared with the results from cyclic voltammetry where a linear trend line of the oxide reduction peak.

The last MFFC had 500 µm electrodes and a channel height of about 100 µm and gave much better results. The electrolyte resistance was calculated from EIS and was reduced a lot to about 300 - 10000 Ω. The cell was tested with a ruthenium red-ox couple (hexaammineruthenium(II)chloride and hexaammineruthenium(III)chloride), and an external hydrogen reference electrode placed in the outlet was found to be simpler to control than an internal reference electrode. The peak separation proved to be depending on the flow rate, and increased with increasing flow rate until the peaks no longer appeared (around 20 µl min^{-1}). At no flow rate, the peak separation decreased with decreasing potential sweep rate.

8 Future work

Future work will be to continue the work of making new flow channels which are much higher than 15 µm. There are a few different photoresists and techniques that can be tried, for instance one of the negative photoresists SU-8 50/100/2100/2150. The photoresist film thickness of the four photoresists varies from 40-550 µm, see Appendix D figures D.2 and D.3. One layer of any of these photoresists will give a much thicker layer, and the channel is higher. It is also possible to apply more than one layer of photoresist to increase the thickness, [27], [28]. Too many layers should probably not be applied, it is better with maybe two to four layers to get the desired thickness, as Mata et al., [28], encountered several problems with their six layer routine. When an appropriate working MFFC is made, key variables like flow rates, potential scan rates, and concentration should be tested with a reversible red-ox system in the electrolyte.

Shielding of subsequent electrodes which means an active component is added to the electrolyte, CO (aq), and the electrolyte is cleansed of this component by applying the appropriate potential to the first electrode. The same potential is applied to the second electrode to reduce what is left. This way, the degree of cleansing is found as a function of flow rate.

Understanding complicated electrode kinetics and reaction mechanisms is very important and this is another application for the MFFC. Also in developing new catalysts, both biological and metallic, especially in biological catalysts where only a small amount are used and the enzymes can only live under certain conditions.

A microfluidic fuel cell should be made from the established routine and the new mask with the fuel cell electrode and channel configuration. The microfluidic fuel cell should be tested with organic species as oxidant, and various electrolyte compositions and then measure cell voltage, power density and fuel consumption. Carbon monoxide (adsorption) on platinum electrodes in sulphuric acid should also be tested.

9 References

[1] E. Kjeang, N. Djilali, and D. Sinton, "Microfluidic fuel cells: A review," *Journal of Power Sources,* pp. 353-369, 2009.

[2] J. Larminie and A. Dicks, *Fuel Cell Systems Explained* second ed.: John Wiley & Sons, 2003.

[3] H. Karoliussen, "Lecture notes in TMT4255 Corrosion and corrosion management - Arbeidsbok 1," 2010.

[4] K. Nisancioglu. (2010). *Lecture notes in TMT4252 Eectrochemistry*.

[5] G. M. Whitesides, "The origins and the future of microfluidics," *Nature,* vol. 442, pp. 368-373, 2006.

[6] E. R. Choban, L. J. Markoski, J. Stoltzfus, J. S. Moore, and P. J. A. Kenis, "Microfluidic Fuel Cells that Lack a PEM," *Power Sources,* vol. 40, pp. 317-320, 2002.

[7] C. J. Geankoplis, *Transport Processes and Separation Process Principles*, Fourth ed. Pearson Education, Inc, 2007.

[8] (2011, 19.10). [Web page].

[9] E. Kjeang, A. G. Brolo, D. A. Harrington, N. Djilali, and D. Sinton, "Hydrogen Peroxide as an Oxidant for Microfluidic Fuel Cells," *Journal of The Electrochemical Society,* vol. 154, pp. B1220-B1226, 2007.

[10] E. R. Choban, L. J. Markoski, A. Wieckowski, and P. J. A. Kenis, "Microfluidic fuel cell based on laminar flow," *Journal of Power Sources,* vol. 128, pp. 54-60, 2003.

[11] A. P. Yadav, A. Nishikata, and T. Tsuru, *Journal of Electrochemical Society*, vol. 156, 2009.

[12] N. Wakabayashi, M. Takeichi, H. Uchida, and M. Watanabe, *Journal of Physical Chemistry*, vol. 109, 2005.

[13] D. Zhang, O. Deutschmann, Y. E. Seidal, and R. J. Behm, *Journal of Physical Chemistry*, vol. 115, 2011.

[14] Z. Jusys, J. Kaiser, and R. J. Behm, *Langmuir*, vol. 19, 2003.

[15] S. Sun, M. Chojak-Halseid, M. Heinen, Z. Jusys, and R. J. Behm, *Journal of Power Sources*, vol. 190, 2009.

[16] E. Kjeang, B. Roesch, J. McKechnie, D. Harrington, N. Djilali, and D. Sinton, "Integrated electrochemical velocimetry for microfluidic devices," *Microfluidics and Nanofluidics,* vol. 3, pp. 403-416, 2007.

[17] A. J. Bard, R. Parsons, and J. Jordan, *Standard potentials in aqeous solutions*. New York: Marcel Dekker, 1985.

[18] C. H. Hamann, A. Hamnett, and W. Vielstich, *Electrochemistry*, Second ed. WILEY-VCH Verlag GmbH & Co. KGaA, Weinheim, 2007.

[19] F. Seland, R. Tunold, and D. A. Harrington, "Impedance study of methanol oxidation on platinum electrodes," *Electrochemical Acta,* vol. 51, pp. 3827-2840, 2006.

[20] B. E. Conway, "Electrochemical oxide film formation at noble metals as a surface-chemical process," *Progress in Surface Science*, vol. 49, pp. 331-338, 370-375, 1995.

[21] (09.11.). *Pine Instrument Company* [Web page].

[22] W. J. Albery and M. L. Hitchman, *Ring-Disk Electrodes*. Oxford University Press: E.W.C. Wilkins & Assoc. Ltd., 1971.

[23] (27.10.). *Pine Instrument Company* [Web page].

[24] S. A.-. Tutorial. (13.06). *Electrochemical Impedance Spectroscopy (EIS): A Powerful and Cost-Effective Tool for Fuel Cell Diagnostics*.

[25] Y. S. Shi, "Electrochemical Microfluidic Device," Univeristy of Victoria Department of Chemistry, 2010.

[26] Microresist.technology. (13.06.2012). *Processing Guidelines - Negative Tone Photoresist Series ma-N 400*.
[27] B. Bohl, R. Steger, R. Zengerle, and P. Koltay, "Multi-layer SU-8 lift-off technology for microfluidic devices," *Journal of Micromechanics and Microengineering,* vol. 15, pp. 1125-1130, 2005.
[28] A. Mata, A. J. Fleischman, and S. Roy, "Fabrication of multi-layer SU-8 microstructures," *Journal of Micromechanics and Microengineering,* vol. 16, pp. 276-284, 2006.
[29] N.-T. Nguyen and S. T. Wereley, *Fundamentals and applications of microfluidics*. Boston: Artech House, 2006.
[30] Microchem. (13.06.2012). *Processing Guidelines - Negative Tone Photoresist Formulations SU-8 2-25*.
[31] Microchem. (13.06.2012). *Processing Guidelines - Negative Tone Photoresist Formulations SU-8 50-100*.
[32] Microchem. (13.06.2012). *Processing Guidelines - Negative Tone Photoresist SU-8 2100 and SU-8 2150*.
[33] F. Vullum-Bruer. (2011). *Lecture notes in TMT4320 Nanomaterials*.
[34] C. Møinichen, "Microfluidic flow cell for studies of electrochemical reactions," Materials Science, NTNU, 2011.
[35] D. Schumann, *Electrochemical Acta,* vol. 35, 1990.
[36] C. Gabrielli and B. Tribollet, *Journal of Electrochemical Society,* vol. 141, 1994.

10 Appendix

A: Calculation of the electrode area

This example is for platinum electrodes in 0.5 M H2SO4, with argon purging. The lower potential limit is 0.05 V and the upper potential limit is 1.6 V. The potential sweep rate is 100 mV s^{-1} and there is no rotation.

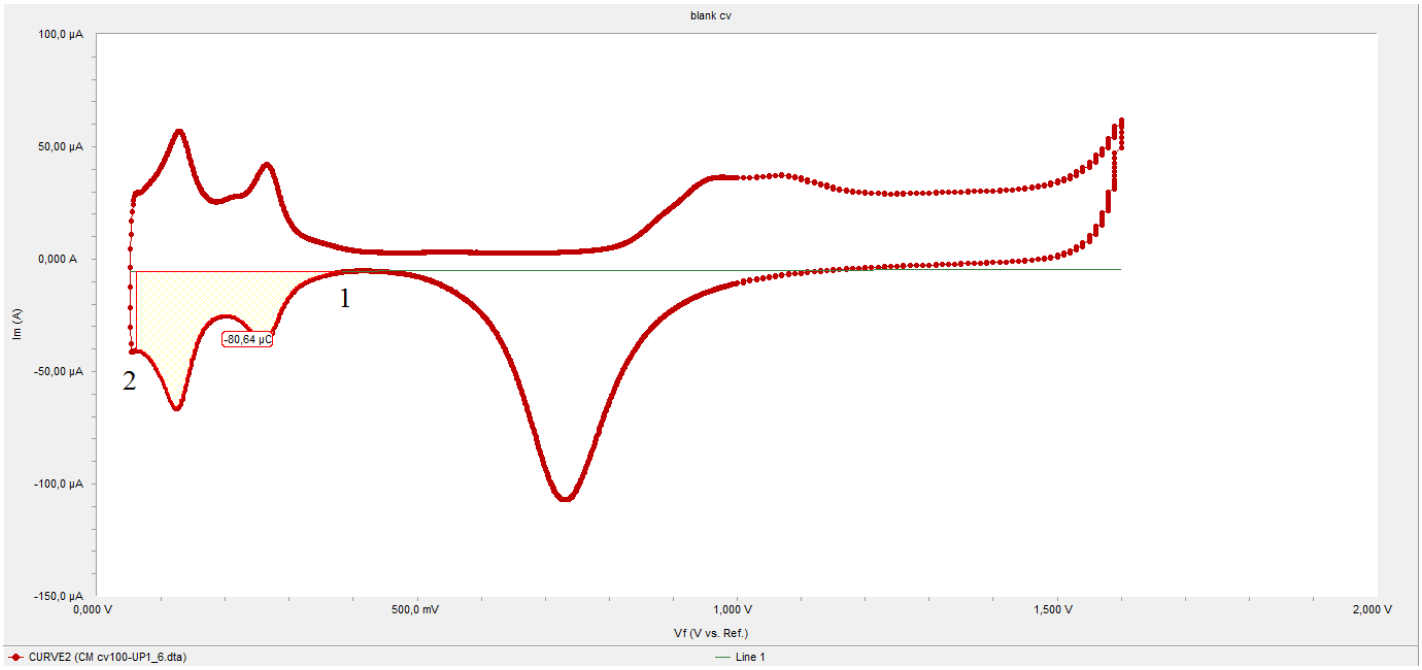

Figure A.1: The voltammogram in the software Echem analyst. The charge of hydrogen adsorbed on the electrode surface is calculated by integrating between the two peaks marked 1 and 2.

The amount of hydrogen adsorbed on the electrode surface is calculated by integrating between the two peaks marked 1 and 2 in figure A.1. The linear line that goes through the voltammogram is added by selecting two points in the flat area and then extrapolate the line.

Here the amount of hydrogen adsorbed was calculated to be -80.64 µC. A monolayer of hydrogen is adsorbed on the electrode surface, i.e. only one hydrogen atom is adsorbed per platinum atom on the electrode surface, see figure A.2. The charge of platinum atoms per cm^2 is 220 µC $cm(Pt)^{-2}$, [19]. The electrode area was calculated by using equation A.1, and was in this example calculated to be 0.37 cm^2.

$$A = \frac{Q_H}{Q_{Pt}} \qquad \text{(A.1)}$$

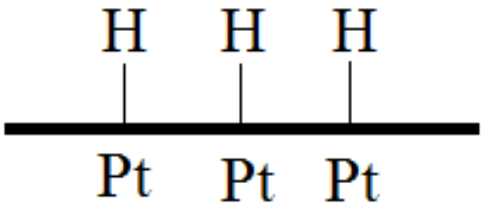

Figure A.2: One hydrogen atom is adsorbed on the electrode surface per platinum atom on the electrode surface.

B: Rotating Ring-Disk Electrode dimensions

Table B.1 Rotating ring-disk electrode dimensions taken from the manufactures web page, [23].

Table B.1: Rotating ring-disk dimensions.

Parameter	**Value**
Disk outer diameter, r_1	4.57 mm
Ring inner diameter, r_2	4.93 mm
Ring outer diameter, r_3	5.38 mm
Collection efficiency	22 %
Disk area	0.1642 cm^2
Ring area	0.0370 cm^2

C: Negative photoresist ma-N 400 series

The ma-N 400 series consists of several photoresists which gives a different photoresist film layer thickness for the same spinning rate. The different spin curves for the different photoresist are shown in figure C.1.

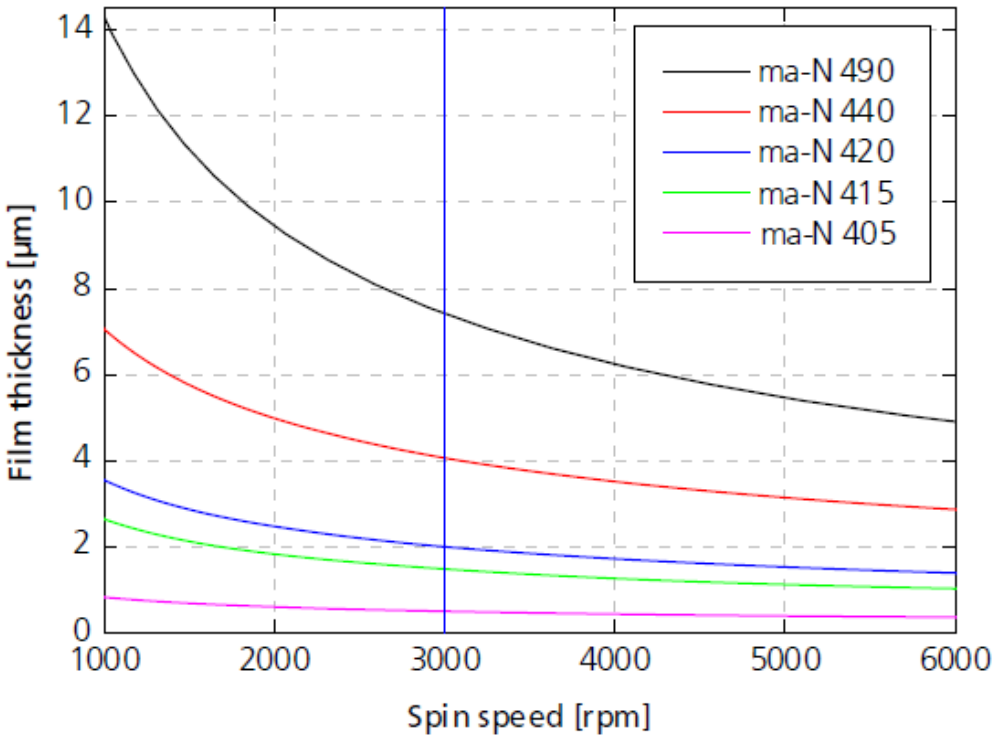

Figure C.1: Spin curves for the negative tone photoresist ma-N400 series, [26].

An undercut profile in the photoresist, after developing, is preferred for metal depositing. The longer the photoresist is developed, the more undercut is the profile, as seen in figure C.2. An undercut profile helps the removal of metal in the lift-off process.

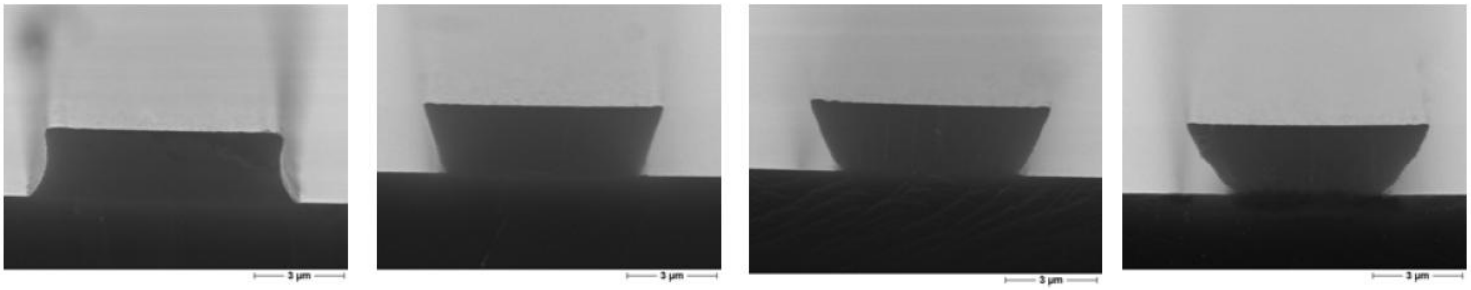

Figure C.2: Undercut profile for 2 µm thick ma-N 400, [26].

D: Negative photoresist SU-8 series

The SU-8 series consists of several photoresists which gives a different photoresist film layer thickness for the same spinning rate. The different spin curves for the different photoresist are shown in figure D.1, D.2 and D.3.

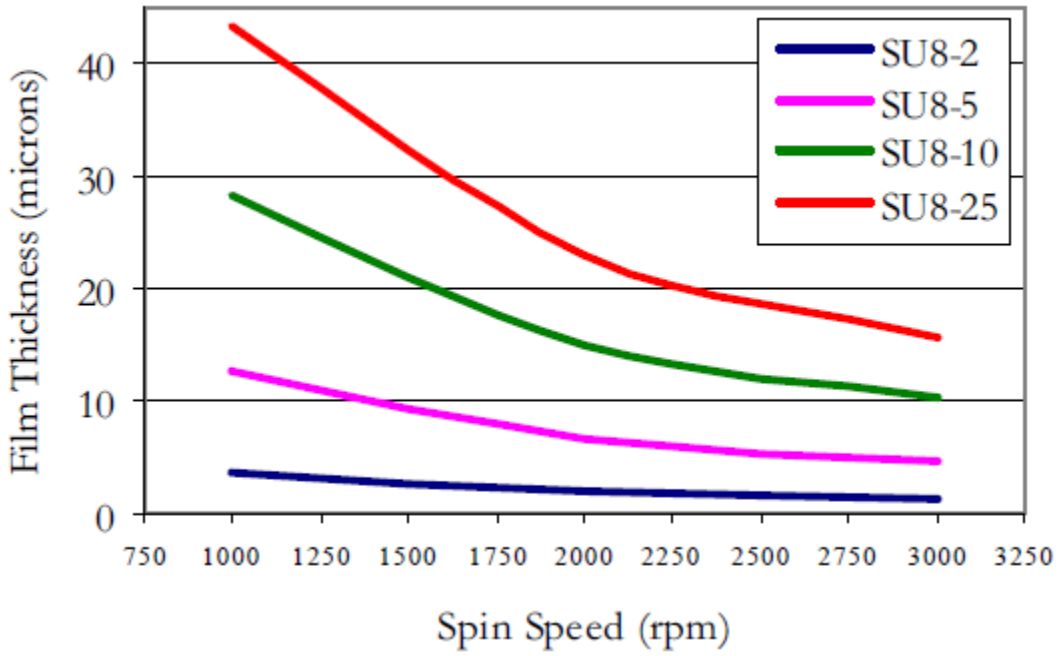

Figure D.1: Spin curves for the negative photoresist SU-8 2-25 series, [30].

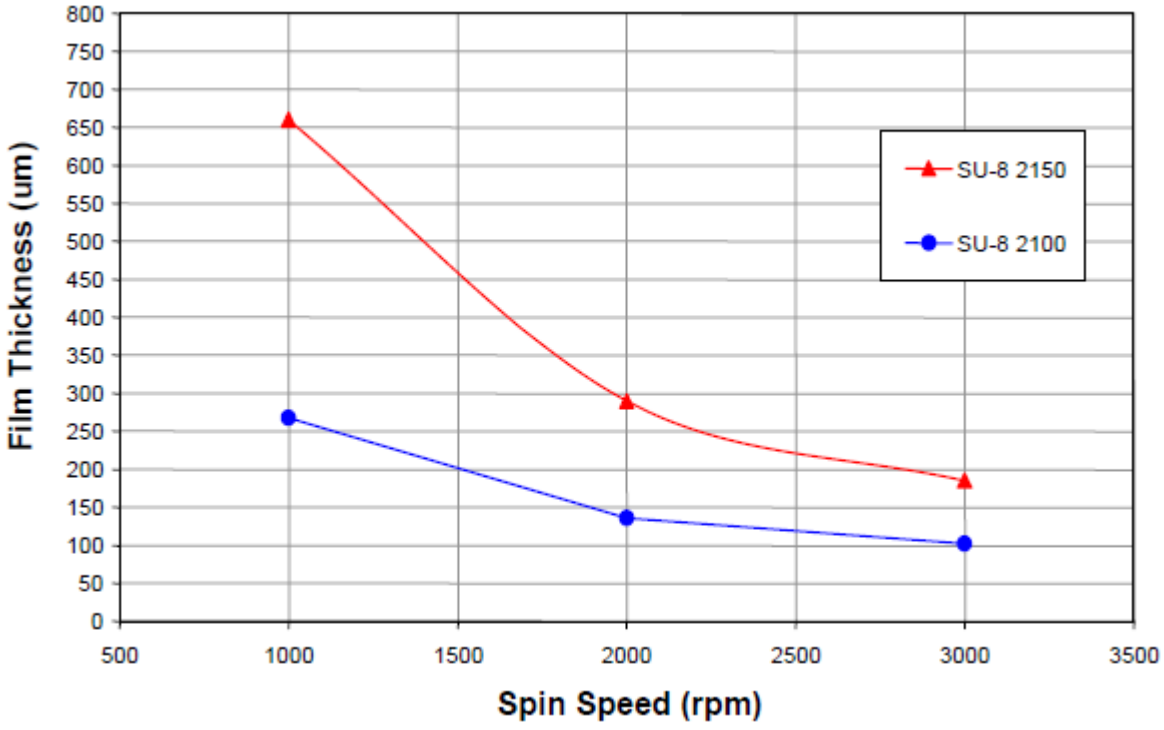

Figure D.2: Spin curves for the negative photoresist SU-8 2000 series, [32].

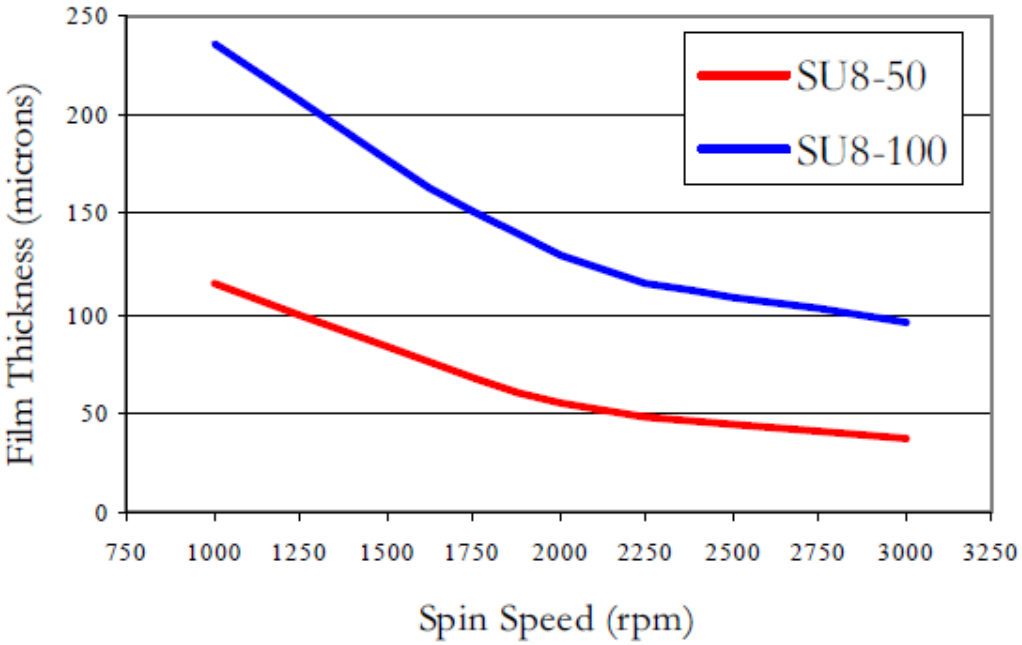

Figure D.3: Spin curves for the negative photoresist SU-8 50-100 series, [31].

The exposure time depends in the photoresist film thickness, and the exposure energy vs. the film thickness is shown in figure D.4.

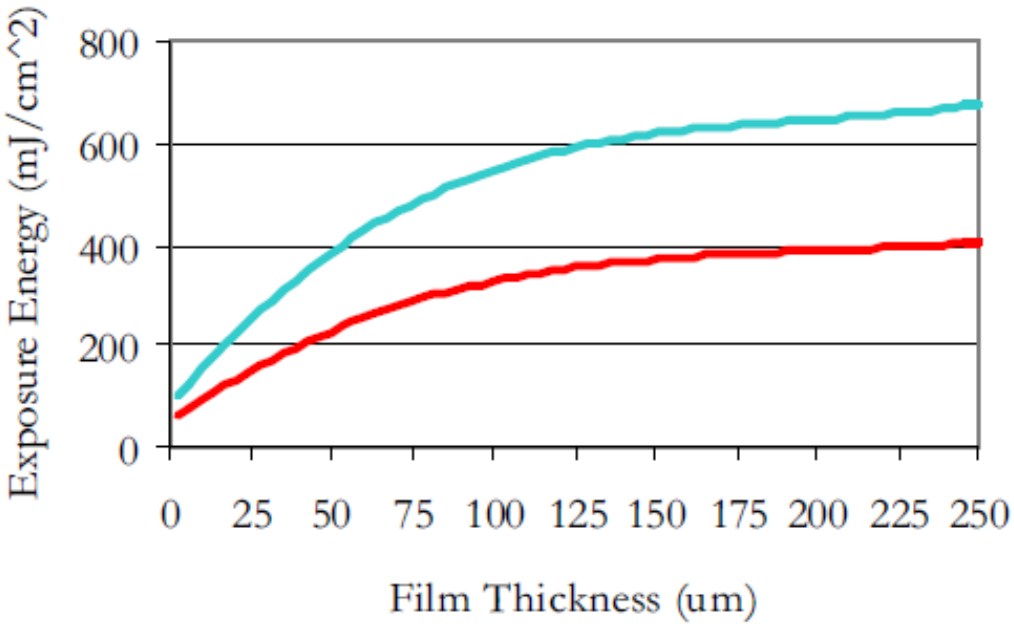

Figure D.4: Recommended exposure dose, [30].

E: Pictures from the procedure of making the MFFCs

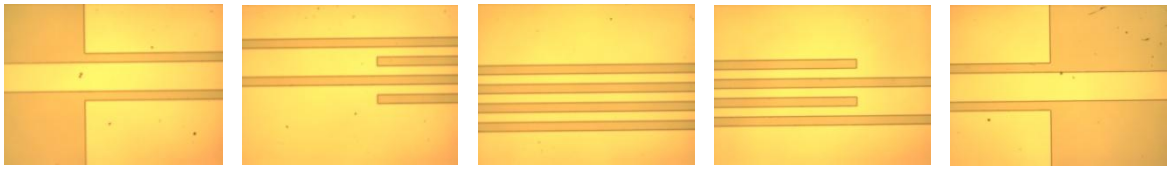

Figure E.1: The electrode area after a successful development. The Photoresist is removed, with an undercut profile.

Figure E.2: The electrode area after metal deposition.

Figure E.3: The electrode area after a successful lift-off process. The metal outside the electrodes is removed.

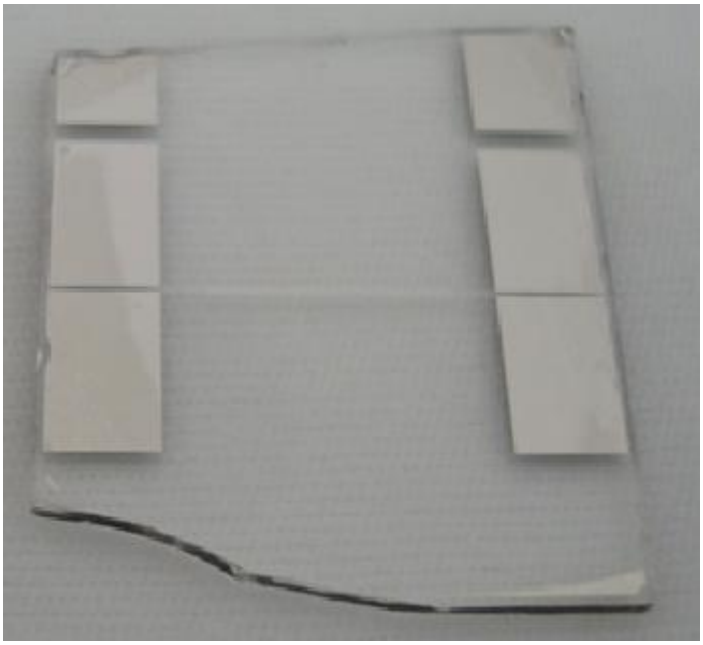

Figure E.4: The glass chip after lift-off, 50 µm wide platinum electrodes.

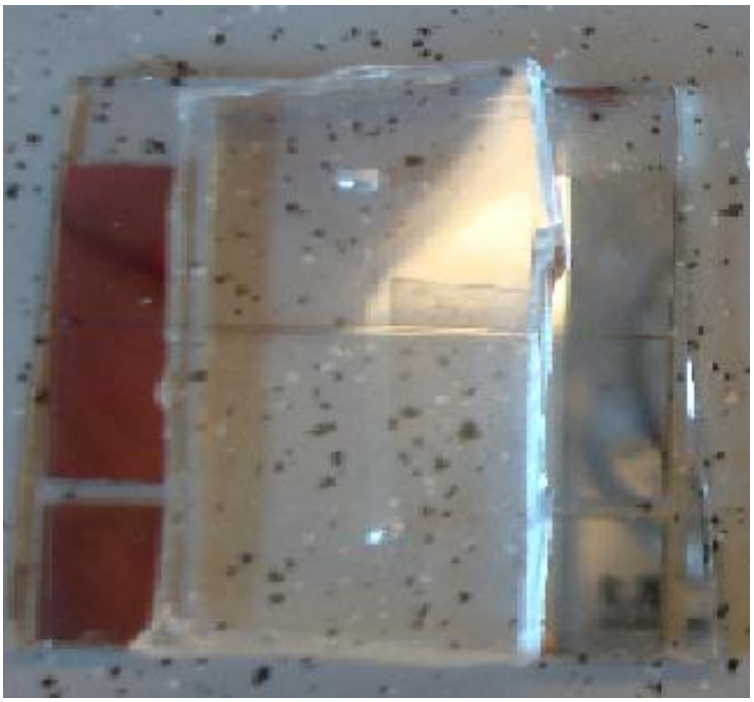

Figure E.5: The glass chip with 50 µm wide platinum electrodes and a 15 µm high flow channel made from an impression in PDMS.

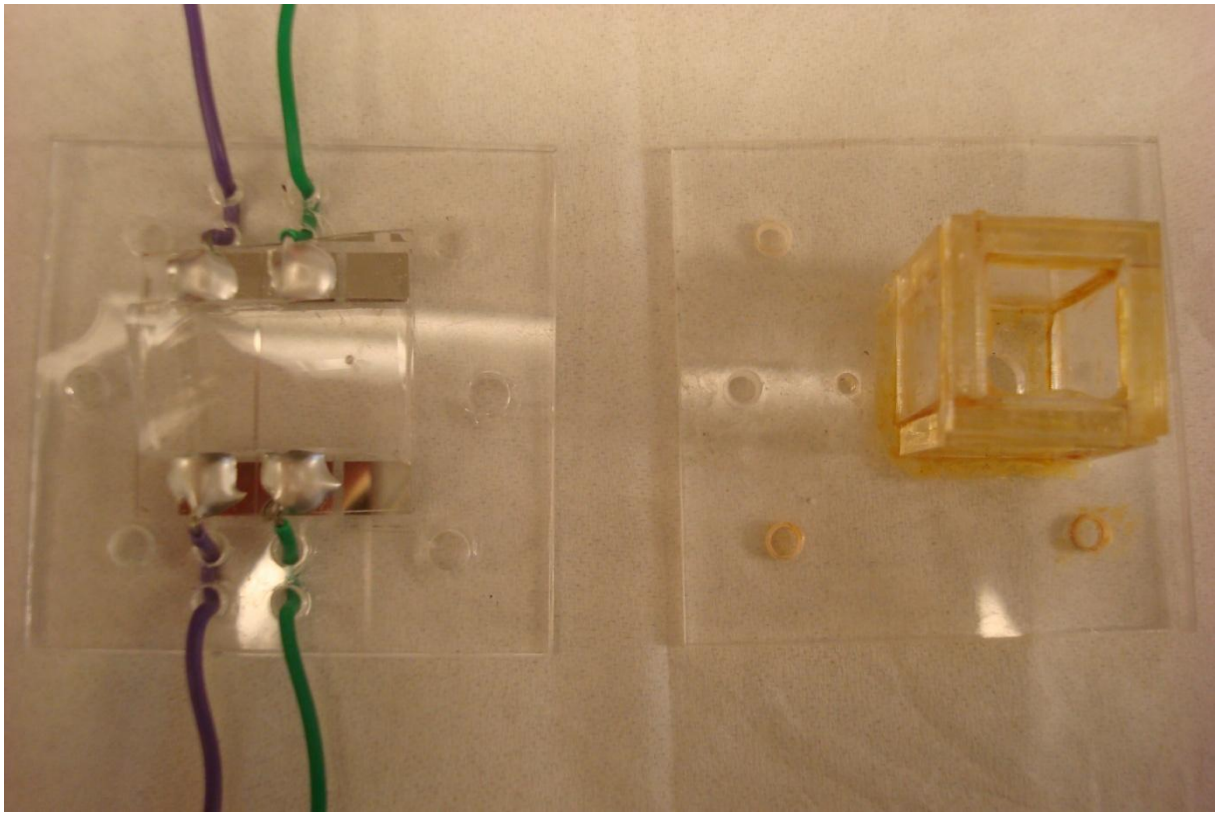

Figure E.6: A finished microfluidic flow cell, including a flow cannel and wires connected to the electrodes. The platinum electrodes are 50 µm wide and the channel width is 1 mm. The plate to the right is attached to the plate to the left with a screw in each corner.